Master's thesis

NTNU
Norwegian University of Science and Technology
Faculty of Information Technology and Electrical Engineering

Georgina Tresanchez Lacorte

Simplified interrogation of a multi-ressonant optical sensor

Master's thesis in Electronic Systems Design
Supervisor: Dag Roar Hjelme
Co-supervisor: Michael Fried
June 2023

NTNU
Norwegian University of
Science and Technology

Georgina Tresanchez Lacorte

Simplified interrogation of a multi-ressonant optical sensor

Master's thesis in Electronic Systems Design
Supervisor: Dag Roar Hjelme
Co-supervisor: Michael Fried
June 2023

Norwegian University of Science and Technology
Faculty of Information Technology and Electrical Engineering

NTNU
Norwegian University of
Science and Technology

ABSTRACT

Optical sensing methods have the capability of offering fast and precise measurements. However, they are not deployed to their full potential because they involve the use of complex equipment, frequent supervision and are complicated to use. For these reasons, industries often choose electronic solutions.

This project aims at demonstrating a new approach to optical sensing. It is based on square wave modulation of a laser that does not require costly equipment and is simple to use. The project was divided in three stages: theoretical demonstration, experimental validation and evaluation.

The theoretical approach introduces the retrieval of the transmission function spectra of a Fabry-Perot interferometer from the injected and transmitted photocurrent and the laser's average wavelength. Secondly, the experimental setup was deployed using a current-modulated laser diode and two photodiodes. An optical spectrum analyzer was used to retrieve the laser's average wavelength. The experiments validated square wave modulation since it was possible to retrieve a satisfactory shape and order of magnitude for the transmission function and a satisfactory shape for the derivative. The method's resolution was also successful and better than current available equivalent optical instruments. Finally, some improvements like raw data fitting and amplitude variations were tested.

In conclusion, this thesis is a contribution to proving square wave modulation as a valid optical interrogation method and gives an insight into future improvements.

ACKNOWLEDGEMENTS

I would like to begin the acknowledgements by expressing my gratitude to my supervisor Dag Roar Hjelme. To begin with, for taking me in as a masters student even though I had a lot to learn from this field. Furthermore, he has also been the intellectual core behind this project and his patience in our discussions (mostly about the project but on Norwegian weather as well) has been invaluable.

Secondly I give my thanks to Michael Fried, who has also been a great help. He introduced me to the lab and was of great support in that area. He has also put his brains into the project and has been essential in the theoretical but also in the practical field. Moreover, he endured my coding mistakes and existential crisis which says a lot about his willingness to help others.

Outside of university I also found good friends that made this exchange semester shine. I am extremely grateful to Arthur, Aina, Christiane, Giacomo, Irene, Josh, Marie, Mees, Simon, Reuben and Vegard for creating long-lasting memories while exploring Norway together and filling my days with laughter. I am also thankful to NTNU and Trondheim for creating such a vibrant atmosphere, which sometimes made it hard to stay working on the master thesis.

Finally I would like to give a warm hug to my parents and family, to whom I owe my education.

CONTENTS

LIST OF FIGURES

ABBREVIATIONS

List of all abbreviations in alphabetic order:

- **AM** Amplitude Modulation
- **ASE** Amplified Spontaneous Emission
- **OSA** Optical Spectrum Analyzer
- **DFB** Distributed Feedback Laser Diode
- **F** Finesse
- **FM** Frequency Modulation
- **FM/AM** FM-generated AM
- **FSR** Free spectral Range
- **LIA** Lock-in Amplifier
- **RAM** Residual Amplitude Modulation
- **SNR** Signal to Noise Ratio
- **WMS** Wavelength Modulation Spectroscopy

CHAPTER

ONE

INTRODUCTION

1.1 Motivation

Optical sensing is considered one of the most sophisticated sensing techniques currently available. However, calibration and testing of optical interrogation methods, such as Wavelength Modulation Spectroscopy (WMS) can be impractical and costly for field-deployable sensors in real-world environments. Additionally, such methods require the use of expensive equipment such as laser swept sources and optical spectrum analyzers, which are more costly than electronic alternatives. Despite these challenges, optical sensing technologies can still compete in a market dominated by electronic solutions due to their ability to resist electromagnetic interference, offer high resolution and sensitivity, and ensure electrical isolation.

The present project aims at bringing the advantages of these optic and electronic solutions into a cost-effective yet high performance method based on square wave modulation. This would eliminate the main reasons that hinder WMS deployment in day-to-day applications and therefore expand its applicability. WMS could be brought to researchers with fewer economic resources as well as industry, since the costs of the setup would decrease drastically.

1.2 Objectives

The main aim of this project is to establish a novel approach for optical interrogation that utilizes a square-wave injection current-modulated laser diode and two photodiodes. The ultimate goal is to eliminate costly materials and complex procedures to achieve a method with similar resolution and sensitivity as WMS. This study was divided in the following targets:

- Demonstrate a novel WMS method using square wave modulation.

- Deployment of a setup for achieving the method.
- Experimental validation of the setup and evaluation.

1.3 Project scope

This project was carried out in the Department of Electronic Systems in the Norwegian University of Technology. It is framed in the strategic research area of ENERSENSE, that is focused on energy efficiency, energy storage and sensor technologies. This project was part of the latter, which offers optical solutions tailored for applications in complex multivariable environments. The findings in this project will be published within this research area and will be used to expand further knowledge around square wave modulation.

CHAPTER

TWO

THEORY

2.1 Optical interrogation

Sensing is the fundamental process by which humans perceive and interact with their environment. Our natural abilities to sense and measure are limited, and as a result, humanity has developed advanced tools and techniques for sensing and measuring beyond our innate capacities.

In almost every scientific discipline, from astronomy to biology to engineering, researchers have developed innovative ways of sensing and measuring the world around us. Photonics, which is the science and technology of generating, controlling, and detecting photons, has been a particularly valuable area for developing new sensing technologies.

Optical interrogation is the name given to a set of optical techniques to obtain information about a physical system. Optical interrogation became feasible with the discovery of optical fibers with low radiation losses [1], optical processing devices [2] as well as adequate light sources and sensors [3]. Montgomery describes this era as the cascade inventions [4], which culminated in the 90s when these technologies stopped being rare lab devices and became available for mass production and implementation. Fiber optics are now an important part of diverse fields such as aerospace [5], civil [6], biomedical [7, 8] and chemical engineering [9].

The rise of optical systems in a market previously dominated by satellite and electrical solutions is due to their superior performance in a number of key areas. One of the primary advantages of optical fibers is that they are electromagnetically passive and made of dielectric materials. This means that they can be safely used in applications with variable electric fields, are highly resistant to high temperatures and are immune to electromagnetic interference. In addition, they offer complete electrical isolation, making them ideal for use in biomedical applications. Moreover, they are highly resistant to chemical and biological agents due to their

silica-based components [10].

Optical fibers also possess a large bandwidth and high sensitivity, and are robust to vibrations and shock. These properties, combined with low loss over long distances and the ability to offer optical and electrical multiplexing, have made optical fibers a critical technology in the field of communications and sensing [10].

Even though optical sensing offers the advantages mentioned above, it still poses some disadvantages in respect to electronic systems. There are many factors that can influence the cost of a sensing technology because each application has its own level of complexity and needs. However, optical detectors and light sources are usually more expensive than their electrical peers. This is because they have a more complex design and require high-tech components, calibration and testing. Moreover, optical elements can sometimes be bulky and less practical to work with. In contrast, electrical circuits usually are more straightforward and easy to implement [11], and are still preferred in many fields.

2.2 Optical systems

This section provides a brief overview of the components in optical systems. For a detailed explanation of each component please refer to Appendix A.

An optical system refers to a collection of objects and components that are designed to control or manipulate light for a specific purpose. In this context, the focus is set on examining optical sensing systems.

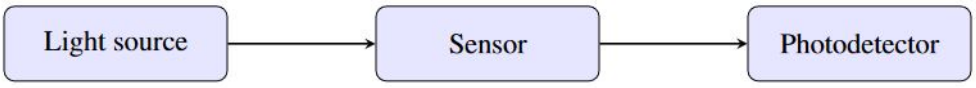

Figure 2.1: The standard setting of an optical system

2.2.1 Light sources

This project relied mainly on two kinds of light sources: lasers and white light sources.

A laser is a light source that runs on stimulated emission and therefore has a highly coherent light beam with a narrow spectral band. For this project a laser with distributed feedback (DFB) was used, since it provides a stable line width and can also be modulated in wavelength.

An important characteristic of lasers is the frequency chirp. It is defined as the change of frequency over time of a laser pulse and it is what this application will take advantage of for obtaining sensing information.

Another important characteristic of DFB lasers is that they may have side modes that can influence measurements. These undesired changes can be triggered by temperature changes or optical feedback from the sensing system. Therefore, it is important to adjust the setup to prevent unexpected shifts in wavelength.

As opposed to lasers, white light sources emit within a broad optical bandwidth with low coherence and high power. In this project they are used for characterizing interferometers and for other equipment checks.

2.2.2 Optical detectors

An optical detector, also known as photodetector, is a device capable of transforming light into a measurable form of energy such as heat or electricity. In this project, only the photoelectric detector application is used, so the term "photodetector" will strictly refer to photoelectric detectors.

Similarly to light emitting diodes, photodetectors are based on the photoelectric effect, but their function is inverse. Instead of emitting photons, the semiconductor material absorbs them, causing electrons to transfer to higher energy levels, which can later be released as an electric current called the photoelectric emission.

2.2.3 Interferometers

An interferometer is an optical instrument that uses the interference of electromagnetic waves to extract information such as temperature, physical strain, imaging, chemical characterisation and many others from a physical system [12].

Their mechanism of operation consists of splitting a light beam in two, one of them is delayed and later recombined with the other. The resulting wave will have an intensity pattern following the superposition principle, and will provide information on the phase and amplitude difference between the two beams [13].

Fabry-Perot interferometer

In this project the transmission function of a Fabry-Perot interferometer is characterized. This interferometer consists in a cavity with two parallel surfaces with semitransparent, highly reflective coatings [14]. The Fabry-Perot is classified as an amplitude-splitting multiple-beam interferometer. When a light beam enters the cavity it is reflected multiple times, which creates an interference pattern that only lets through the wavelengths that are resonant with the cavity.

The parameter for evaluating the Fabry-Perot's performance is the finesse (F). Higher finesse values give sharper transmission windows that are easier to locate while low-finesse ones have flatter transmission profiles over wider wavelength ranges [11]. Figure 2.2 presents some Fabry-Perot transmission spectra with different finesse values. This spectra can be expressed with the Airy distribution, but each peak can be fitted into a Lorentzian curve.

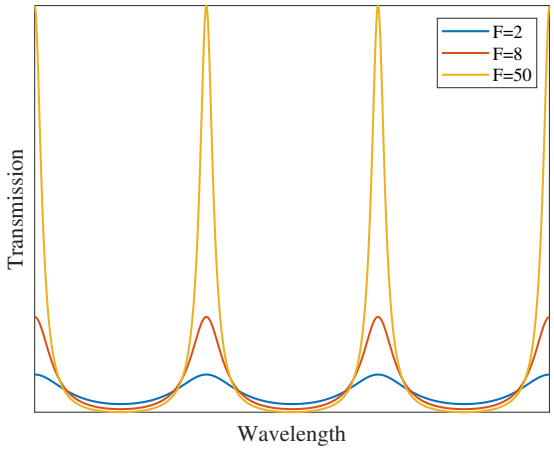

Figure 2.2: Fabry-Perot transmission for different finesse values.

Another important parameter is the free spectral range (FSR), which denotes the distance between the transmission peaks of the Fabry-Perot interferometer. It depends on the refractive index and distance between mirrors.

The main reason why this interferometer was selected is that the ressonant wavelength of the Fabry-Perot can be changed through voltage. This means that a Fabry-Perot has a low time constant, unlike interferometers that rely on temperature such as Fiber-Bragg gratings. However, Fabry-Perots are sensitive to temperature changes and need to be coupled with a temperature controller to minimize such fluctuations during measurements. Temperature affects the refractive index and expansion of the medium between the mirrors, bowing and reflectivity of the reflector and scattering in the medium, which will distort the transmission spectra.

2.2.4 Noise in optical systems

Noise is the term used to refer to unwanted random fluctuations of a signal. In photonics, and particularly in precision applications, noise has a profound impact and an adequate noise reduction is key for correct sensing. In this section noise is characterized in individual components as well as the system as a whole.

Noise in laser sources

Laser noise has an impact on the intensity, frequency, and phase of the laser's output. Despite operating based on stimulated emission, lasers can also generate photons through spontaneous emission, which is random, broadband, and multi-directional. These spontaneously emitted photons can be amplified within the laser cavity, leading to a phenomenon known as amplified spontaneous emission (ASE) [15]. ASE introduces side-modes and relaxation oscillations, which can disrupt the laser's intended operation. Apart from internal noise, lasers are also susceptible to optical feedback, which causes interference that leads to mode hopping and linewidth broadening [15].

The quality in the construction of the laser is key in guaranteeing stability. Reducing noise in lasers can be achieved by operating the laser with the adequate parameters. Additionally, the system's feedback can be reduced by using circulators or long fibers.

Noise in photodetectors

There are five main sources of noise in photodetectors, listed by Saleh in Fundamentals of Photonics [15].

1. *Photon noise:* Photons reach the photodetector randomly and therefore the input is governed by a Poisson distribution.

2. *Photoelectron noise:* The efficiency of the photodetector is never one, meaning that every single photon does not create one electron. Since this events occur randomly, it is a source of noise.

3. *Gain noise:* The amplification mechanism and the bias applied to the photodetector can provide different gain values for carriers.

4. *Receiver circuit noise:* The electrical components that are in charge of receiving and analyzing the signal also contribute to noise.

5. *Dark currents:* In the absence of light, photodetectors can also create currents of electrons generated thermally of through tunnelling.

General noise sources

Optical circuits as a whole are also subject to environmental factors that create noise. Thermal noise can cause fluctuations in the system because of its influence on the refractive index of some materials and the expansion and contraction of the transmitting media. Avoiding thermal noise can be achieved by maintaining a regular room temperature and cooling some optical components.

Mechanical vibrations are another source of environmental noise, since it affects the stability of the setup. Vibrations can be seen as sharp peaks in the noise spectrum, and they can be mitigated by separating cooling systems and other machines as well as having a robust setup.

2.3 Wavelength modulation spectroscopy

WMS is an optical sensing technique that uses a laser to probe the absorption features of a sample [16]. In WMS, the laser's wavelength is modulated sinusoidally at a fixed frequency while it is tuned across the absorption features of the sample. This allows the laser light to interact with the sample's absorption line, resulting in a complex signal containing both intensity modulation and several harmonics from the modulation frequency [17].

Extracting information from a WMS spectra is quite complex, and extensive work on its analytical background has been developed. However, WMS gives laser

sensing its full potential by posing two main advantages in respect to traditional absorption spectroscopy. The first one is that the signal is only dependent on changes in the sample's transmissivity with wavelength, which means that there is no need to compare measurements with absence and presence of the analyte. The second advantage is that sensing is made at high frequencies, which offers high detectability because $1/f$ noise is drastically minimized [18].

Wavelength modulation spectroscopy is mainly used in gas characterizations. The technique is able to provide non intrusive measurements of gas temperature, pressure, composition and velocity [19]. Because it is able to offer the robustness to harsh environments of an optical system, it is widely used for flame monitoring and combustion diagnostics [20] as well as industrial process control [21]. Moreover, it has found applications in the biomedical field for trace gas sensing [22] and total viable counts in microbiology [23].

2.3.1 Basic principles

This section aims at introducing the reader to WMS and setting a common ground for nomenclature. It is mostly based on the article by Kluczynski et al. [17], readers who wish to gain a deeper insight in WMS can refer to it for a thorough description.

WMS is based on three main stages:

- Modulation of the laser wavelength with the injection current. The modulation needs to go through the sample's absorption feature as well as sweep through different wavelengths.
- Interaction between the light and the sample, the interaction will interfere with the beam and create a complex signal.
- Detection of the resulting signal with a lock-in amplifier that can extract information on the nth harmonics.

Modulation of the laser wavelength is done by ramping the laser wavelength through the absorption feature and simultaneously adding a harmonic modulation at the injection current. The current fed to the laser with a modulation amplitude of Δi and a frequency f is as follows.

$$i(t) = i_0 + \Delta i \cos(2\pi f t) \tag{2.1}$$

Where $i(t)$ is the injection current and i_0 the bias current. The corresponding frequency output is described by a similar equation.

$$\nu(t) = \nu_0 + \Delta\nu \cos(2\pi f t + \psi) \tag{2.2}$$

Where ν_0 is the laser central frequency and $\Delta\nu$ the frequency modulation (FM) amplitude. The relationship between the two variables is determined by the linear laser injection current-to-frequency response $\kappa_{\nu,ic}$.

$$\Delta\nu = \kappa_{\nu,ic} \cdot \Delta i \tag{2.3}$$

The modulation in the injection current will also create a simultaneous modulation in the laser's light intensity $I(t)$, around a central I_0 and with an amplitude of ΔI.

$$I_{LD}(t) = I_0 + \Delta I \cos(2\pi f t) \tag{2.4}$$

This intensity modulation, also known as Residual Amplitude Modulation (RAM) is an undesired effect that distorts the signals and its magnitude is associated with laser configuration, which requires calibration and tests before measuring.

Once the beam exits the laser it goes through the analyte. The interaction of the sample with the light beam is defined by Beer-Lambert's Law [24].

$$I_{out} = I_{in} e^{-\alpha(\nu)Cl} \approx I_{in}[1 - \alpha(\nu)Cl] \tag{2.5}$$

$\alpha(\nu)$ refers to the absorption profile at frequency ν, C is the concentration expressed as molecular density and l is the length of the interaction. The approximation is only valid for small $\alpha(\nu)Cl$. Since this response is non-linear, there will be some extra amplitude modulation (AM) due to the ν modulation at multiples of the modulation frequency. These terms are referred to as FM-generated AM (FM/AM).

Finally, the detected signal is picked up by a lock-in amplifier (LIA) that compares a reference arm with the sample signal [25]. The generated output is the first and second harmonic of the signal I_{out}, which are proportional to the first and second derivative of the transmission spectra [26]. The following equations describe the first and second harmonic components [27] .

$$\begin{aligned} I_{1f} = \Delta I \cdot \cos(\omega t) - \Delta I \cdot \alpha(\nu_c) \cdot Cl \cdot \cos(\omega t) \\ -\Delta\nu \cdot I_c \cdot \alpha'(\nu_c) \cdot Cl \cdot \cos(\omega t - \psi) \end{aligned} \tag{2.6}$$

$$\begin{aligned} I_{2f} = -\frac{\Delta\nu}{2} \cdot \Delta I \cdot \alpha'(\nu_c) \cdot Cl \cdot \cos(2\omega t - \psi) \\ -\frac{\Delta\nu^2}{4} \cdot I_c \cdot \alpha''(\nu_c) \cdot Cl \cdot \cos(2\omega t - \psi) \end{aligned} \tag{2.7}$$

Where $\Delta\nu$ and ΔI are the FM and AM amplitudes. The phase shift between AM and FM is noted by ψ and it is a function of the modulation frequency f, where, $\omega = 2\pi f$. It must be noted that these equations are only valid for small modulation indexes $m = \frac{\Delta\nu}{\nu_c} < 0.2$ [28].

Extracting the absorption signal from the equations in WMS is a complex task due to the varying values of parameters associated with the laser such as I_0, ΔI, $\Delta\nu$, ψ and ν_c. These parameters can change unexpectedly over time due to various factors such as laser aging, optical fiber loss, or misalignment [27], which makes it crucial to characterize them before each measurement. However, in industrial settings, this can be inconvenient as it requires frequent assistance. Therefore, the need for a setup that can run unsupervised for an extended period of time makes calibration-free systems relevant.

2.3.2 Alternative perspectives to WMS

In this section, three alternative approaches to WMS are presented. The first two are calibration-free systems while the third one is a simplified version of WMS.

The aim of callibration-free WMS systems is to retrieve the absorption signal of a sample without having to pre-characterize the laser's features and thus run unsupervised. The methods are thoroughly demonstrated in the article by Behera *et al.* [27].

Nevertheless, these setups require expensive equipment and complicated additional information such as the phase shift between RAM and FM/AM modulations. Therefore, a simplified approach based on dual wavelength differential detection, based on Ouellette *et al* [29] is also presented.

Background RAM estimation

RAM estimation consists of isolating terms that have the ψ phase shift in the first harmonic, the last term in equation (2.6), and estimate the RAM baseline through the whole spectra using the non-absorbing ends of the function. The isolation of the curve with phase shift can be achieved with an adequate tuning of the LIA phase selection [30] and other methods. It is possible to obtain $1 - \alpha(\nu_c)Cl$ by dividing the measured signal by the estimated RAM.

The technique was successfully proven for measuring gas concentrations [31] and showed errors in the transmission function up to 2.76% with modulation indexes of $m < 0.2$. Even though this technique does not have the inherent low noise levels of traditional WMS, results showed that it is possible to keep signal strength by applying a correction algorithm that takes into account second-order derivative terms.

The drawbacks of this method are that if the sample has other gases with nearby absorption peaks, the estimated RAM spectra will be incorrect. Also, the scanning range needs to be wide as it has to frame the target spectra as well as its non-absorbing ends. Having a wide wavelength range is inconvenient because the laser parameters are often non-linear through frequency and therefore the estimation will not be accurate through the bandwidth.

First harmonic normalization

The second method, first harmonic normalization, takes advantage of an estimation of the first harmonic signal amplitude as $R_{1f} \approx 0.5\Delta I$ at low optical depths and assuming there are zero FM/AM contributions. The higher harmonics are normalized with ΔI, which will eliminate all common perturbances. The advantage of this method is that it offers real-time calibration and eliminates RAM contributions efficiently. However the assumption that FM/AM can be neglected is not always true since FM/AM contributions are significant when $\Delta I/I$ is small.

This method was also tested for measuring gas conditions [32] and displayed a 95% confidence interval, with errors as low as 0.32% in transmission peaks with

modulations of $0.1 < m < 0.5$

Dual wavelength differential detection

This method was developed using a fiber Bragg Grating, which is a ressonant sensor that has a transmission spectra that can be assimilated into a Gaussian curve. The objective of the method is to retrieve the central wavelength λ_B of this curve.

To do so, a laser is modulated with a square wave, which in turns creates a frequency chirp. By doing a full characterization of the chirp, the authors could link time with a specific wavelength. The key to finding the λ_B is selecting two time instants that give two wavelengths λ_+ and λ_- separated by a distance δ. By measuring the reflected power at the same instants (P_+ and P_-) it is possible to obtain:

$$S = \frac{P_+ - P_-}{P_+ \cdot P_-} = 4 \ln 2 \frac{\delta}{\omega_B^2} \cdot (\lambda_B - \lambda_{av} \tag{2.8}$$

Where ω_B^2 is the grating's full width at half maximum and λ_{av} is the average of λ_+ and λ_-. S is dimensionless, linearly related to the difference between λ_{av} and λ_B and is insensitive to transmission loss between the source and the grating, as long as it remains constant through time.

The authors obtained a resolution of 0.05 pm, that is limited by the smallest power difference that can be detected. In turn, this is subject to noise in photodetectors, laser power and analogue-to-digital converter. The obtained resolution is one of the main strong points of the method, along with its low cost and simplicity. However, the technique is subject to laser stability as the dynamic chirp is the main reference for λ_B.

2.3.3 Square wave modulation

The method presented in this project, square wave modulation WMS, is a calibration-free spectroscopy technique that only requires a tunable laser diode, a photodetector and an OSA. Therefore, it offers the practical advantages of a calibration-free system in a low-cost setup. This section is a theoretical derivation of the method, that is assessed by trying to estimate the transmission spectra of a Fabry-Perot interferometer. The key of this method is the modulation of the laser with a square wave and taking advantage of the symmetry in the dynamic frequency chirp.

The intensity of the photocurrent of the laser diode, modulated with a square wave $m(t)$ with a period T is:

$$I_{LD}(t) = I_0 + \Delta I_m \cdot m(t) \tag{2.9}$$

The frequency this laser displays will be given by the dynamic frequency chirp $\Delta\nu_m g(t)$, where $g(t)$ can also be expressed as a multiplication of the square wave with a function $h(t)$, as depicted in figure 2.3.

$$\nu_{LD}(t) = \nu_0 + \Delta\nu_m \cdot g(t) = \nu_0 + \Delta\nu_m \cdot h(t) \cdot m(t) \tag{2.10}$$

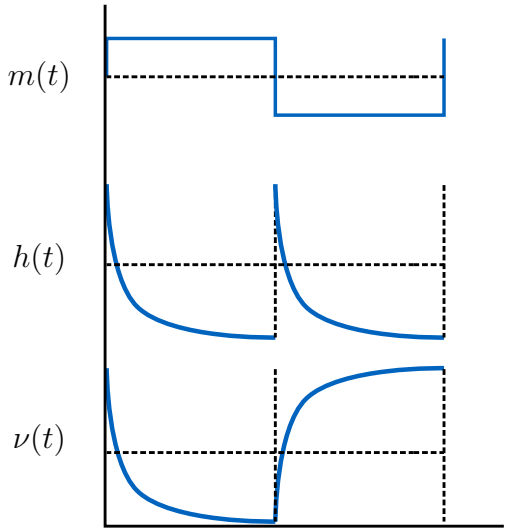

Figure 2.3: The laser chirp $\nu(t)$ expressed as a function of the intensity modulation $m(t)$ and an ideal function $h(t)$

The main observation from the figure above is that $h(t)$ is the same function for every half period, meaning that the laser behaviour remains the same regardless of the transition direction, whether if it's moving from high to low or vice versa. This means that adding the points that are separated by $(T/2)$ will yield a constant value because their separation from the high and low value will be the same, giving the behaviour of the laser at a unique frequency.

The proposed method takes advantage of this property by scanning the square wave modulation of the laser across a Fabry-Perot, as seen in Figure 2.4 (a). The Fabry-Perot's central frequency is moved at a much slower rate than the laser and so each pulse can be considered to go through a specific transmissivity,

After going through the Fabry-Perot, the resulting intensity (Figure 2.4 (b)) will have varied according to its transmission spectra $\mathscr{L}(\nu)$ that is described by a Lorentzian curve with a resonance frequency of ν_{FP} and a linewidth $\Delta\nu_{FP}$.

$$I_{FP}(t) = I_{LD} \cdot \mathscr{L}(\nu_{LD}(t)) \tag{2.11}$$

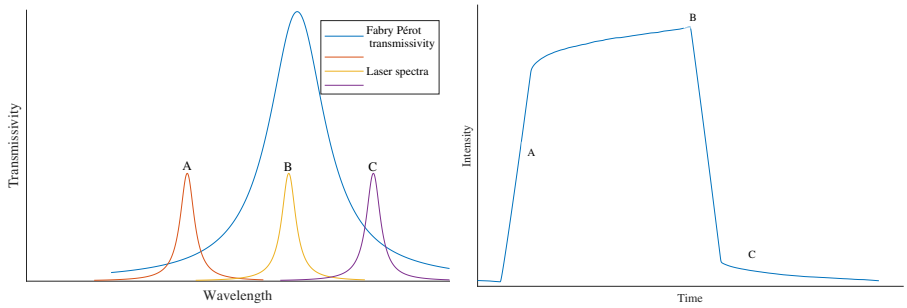

(a) **(b)**

Figure 2.4: **(a)** Fabry-Perot spectra with three laser positions. **(b)** Intensity output through time after sweeping the laser through the Fabry-Perot with the three corresponding positions seen in the left.

When the laser modulation is much smaller than the linewidth of the Fabry-Perot, $\Delta\nu_m/\Delta\nu_{FP} << 1$, the equation above can be approximated into:

$$\begin{aligned} I_{FP}(t) &\approx I_{LD}(t) \cdot [\mathscr{L}(\nu_0) + \mathscr{L}'(\nu_0) \cdot \Delta\nu_m \cdot g(t)] \\ &= [I_0 + \Delta I_m \cdot m(t)] \cdot [\mathscr{L}_0 + \mathscr{L}'_0 \cdot \Delta\nu_m \cdot g(t)] \\ = I_0\mathscr{L}_0 + \Delta I_m\mathscr{L}_0 m(t) &+ I_0\mathscr{L}'_0\Delta\nu_m h(t)m(t) + \Delta I_m\mathscr{L}'_0\Delta\nu_m h(t) \end{aligned} \tag{2.12}$$

In order to get two symmetric signals, the signal is sampled at t_s and $t_s + T/2$, where m(t) takes the values $m(t_s) = 1$ and $m(ts + T/2) = -1$, which are the top and low part of the pulse, as can be seen in the image below (2.5). Following this, the signals are added and subtracted to obtain I_+ and I_-.

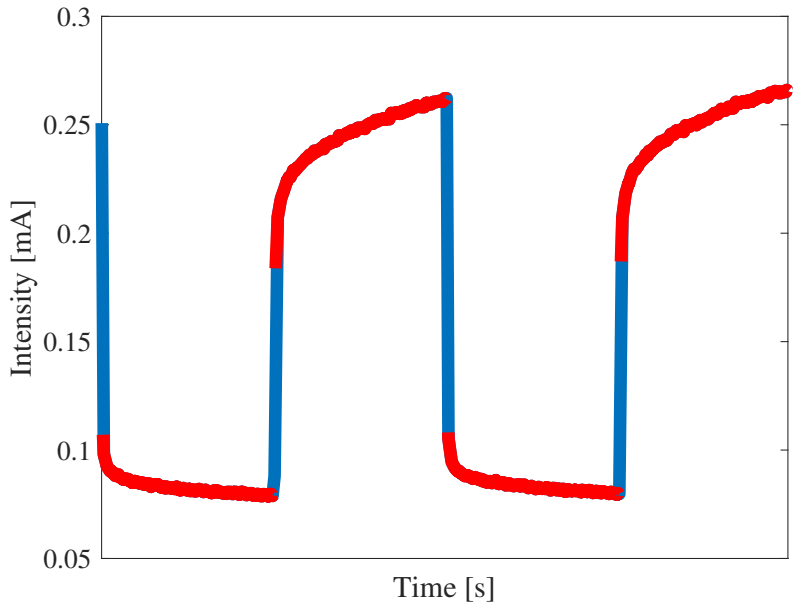

Figure 2.5: Shape of a two pulses, red points indicate the selected ranges for calculating I_+ and I_- while blue ones were discarded.

$$\begin{aligned} I_+ &= I_{FP} + I_{FP}(ts + T/2) = 2[I_0\mathscr{L}_0 + \Delta I_m\Delta\nu_m\mathscr{L}'_0 h(t_s)] \\ I_- &= I_{FP} - I_{FP}(ts + T/2) = 2[\Delta I_m\mathscr{L}_0 + I_0\mathscr{L}'_0\Delta\nu_m h(t_s)] \end{aligned} \tag{2.13}$$

These equations can be rearranged in the following matrix equation, and the Lorentz terms can be isolated. Furthermore, intensity parameters are normalized $i = I_m/I_0$ and averaged over $T/2$, denoted by $< \cdot >$. For the full derivation refer to appendix B.

$$\begin{pmatrix} \mathscr{L}_0 \\ \mathscr{L}'_0\Delta\nu_m < h(t) > \end{pmatrix} = \frac{1}{2(1 - \Delta i_m^2)} \begin{pmatrix} 1 & -\Delta i_m \\ -\Delta i_m & 1 \end{pmatrix} \begin{pmatrix} < i_+ > \\ < i_- > \end{pmatrix} \tag{2.14}$$

From this equation it is easy to identify the parameters that have to be calculated during the measurements: the photocurrent intensity modulation depth $\frac{\Delta I_m}{I_0}$, the

intensities I_+ and I_- and the average frequency shift on half a cycle $< h(t)\Delta\nu_m >$. It can be seen that the only parameter that is not immediate is the frequency shift.

To calculate $< h(t)\Delta\nu_m >$, it is necessary to take into account the energy within the measured frequency band $E(\nu)$, which is defined as $E(\nu) = P \cdot dt = P\frac{dt}{d\nu} \cdot d\nu$. The spectral density will therefore be $S(\nu) = \frac{E(\nu)}{d\nu}$ and for one cycle it is $S(\nu) = P_+\frac{dt}{d\nu} + P_-\frac{dt}{d\nu}$. From this we can extract the average frequency following:

$$< \nu >= \frac{\int \nu S(\nu)}{\int S(\nu)d\nu} \approx < \nu_+ > + < \nu_- > \tag{2.15}$$

A visual representation of this can be observed in the lowest plot of Figure 2.3, where drawing a horizontal line at any frequency value reveals that each cycle has two contributions to that value, one in each half period. These two values are expressed in relation to the equation defining the laser's behaviour 2.11 as:

$$< \nu_\pm >= \frac{[\frac{T}{2}\nu_0 \pm \frac{T}{2}\Delta\nu_m < h(t) >] \cdot [P_0 \pm \Delta P]}{\int S(\nu)d\nu} \tag{2.16}$$

The complete derivation can be found in Appendix B. If the two terms are added the resulting average frequency is defined as follow.

$$< \nu >= \frac{TP_0[\nu_0 + \frac{\Delta P}{P_0}\Delta\nu_m < h(t) >]}{\int S(\nu)d\nu} \tag{2.17}$$

Where $< h(t) >= \frac{2}{T}\int_0^{T/2} h(t)dt$ and $\int S(\nu)d\nu = \int Pdt = T \cdot P_0$ and so the final average frequency is:

$$< \nu >= \nu_0 + \frac{\Delta P}{P_0}\Delta\nu_m < h(t) > \tag{2.18}$$

From this, $\frac{\Delta P}{P_0}$ can be assimilated into Δi_m, as it is the same ratio. $\Delta\nu_m$ and ν_0 can be extracted from measuring the laser's spectra with presence and absence of modulation with a spectrum analyzer. Finally, the average frequency shift is then given by:

$$\Delta\nu_m < h >= \frac{< \nu > -\nu_0}{\Delta P/P_0} \tag{2.19}$$

CHAPTER

THREE

METHOD DEVELOPMENT

3.1 Experimental setup

The figure below illustrates the proposed experimental setup. The wave generator used to modulate the laser diode will be referred as wave generator LD and the one used for the Fabry-Perot as wave generator FP.

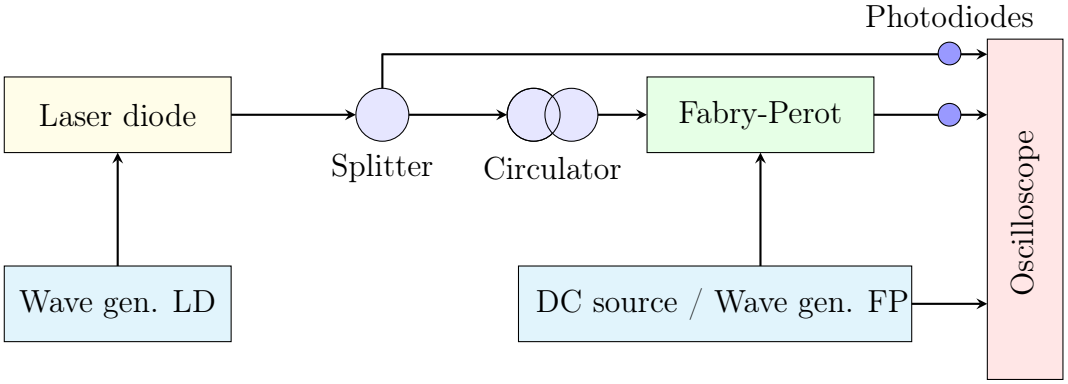

Figure 3.1: Diagram of the proposed setup.

The specific components and channel settings can be found in Appendix C. After setting up the experimental apparatus, a verification process was carried out in two stages: characterization of optical components and study of their stability.

3.1.1 Characterization of the optical components

The aim of these measures was to assess the compatibility of the laser with the different available Faby-Perots. The laser has two parameters that can be adjusted: intensity input and temperature. An increase in intensity will yield more power and shift the resonance wavelength slightly to longer wavelengths. The intensity

needs to be as far as possible from the threshold value and strong enough to be detected without saturating the photodetectors. Temperature also affects the wavelength, higher temperatures shift the average wavelength to the right. It is important to keep the temperature to a low value, similar to room temperature, to prevent fluctuations of the controller. Therefore, the temperature was set at 15 °C.

The studied spectra was represented with logarithmic scaling to keep track of the side modes, to prevent the effects mentioned in Section 2.2.1.

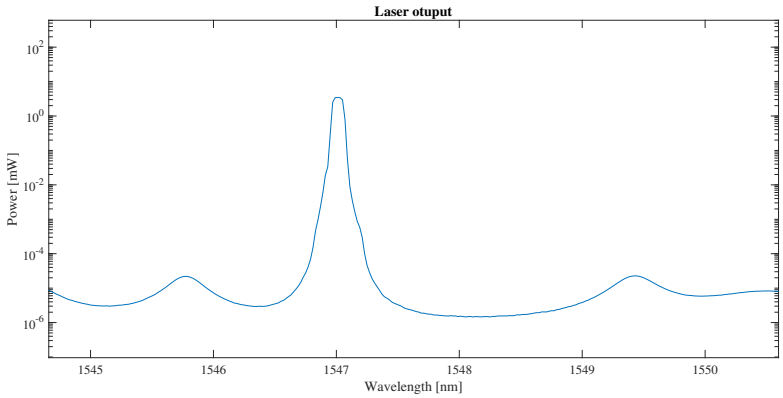

Figure 3.2: Measured laser spectra with the temperature set at 15 °C and the intensity at 17 mA.

The Fabry-Perot selection was based on the one that had the least free spectral range, meaning that the resonance peaks were closer to each other and the laser would be easier to tune with. Even though the Model 1983 was the one that fulfilled this requirement best, it had some operational problems so the selected one was 7447.

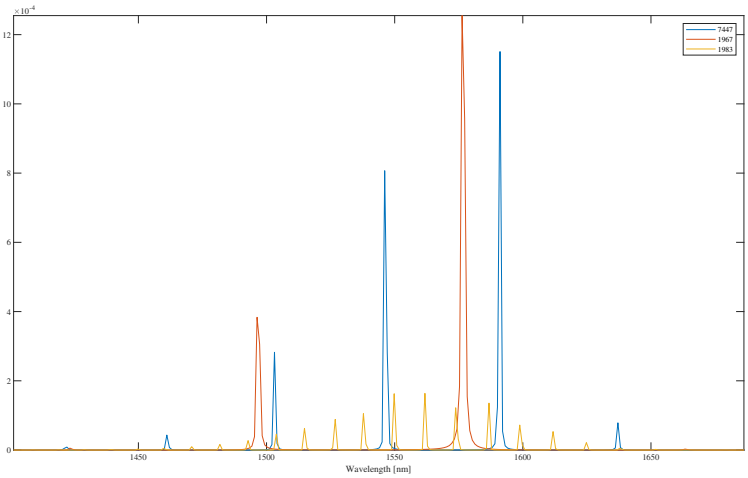

Figure 3.3: Fabry-Perot resonance measured with a white light source and an OSA.

3.1.2 Stability of optical components

The method to evaluate the stability of the optical components was to record their spectrum using an OSA periodically during the study period. Once the data was collected, each optical spectrum was fitted with a Lorentz curve, from which the parameters of the central wavelength and maximum power were extracted. These values were then represented through time to assess any fluctuations.

The studied components were the laser, the white light source and the Fabry-Perot. The reason why the white light source was also studied, even though it is not involved in the experimental setup, is that it was used to get the Fabry-Perot spectra, and therefore could also be a source of instability. The recording started immediately after the equipment was turned on and lasted for one hour.

The laser was found to have satisfactory results, once stabilized, the maximum wavelength drift was 0.004 nm with a power change of 0.114 mW. In Figure 3.4 (a) it can be seen that it had a warm up time of about 40 minutes for wavelength. The white light source also had a stable output, it was measured at the wavelength that was used to scan the Fabry-Perot later on. The peak drifted 0.13 nm in wavelength and 22.1 nW in optical power.

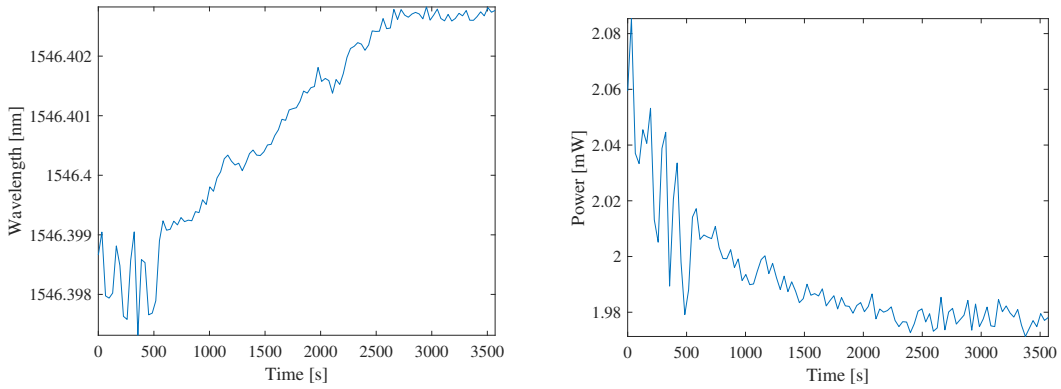

Figure 3.4: **(a)** Laser diode: maximum power wavelength through time. **(b)** Laser diode: maximum power through time.

For the Fabry-Perot, stability was also satisfactory, but it was seen that the DC source did fluctuate in certain regions, changing the resonance wavelength. Therefore, another assessment was carried out to determine if the DC source was an adequate controller for the Fabry-Perot by reading the transmission output with a long recording time of the oscilloscope. The DC source output was increased 0.01 V every 120 seconds. It can be clearly seen in Figure 3.5 that the signal is noisy, that the steps in the DC source are not regular and that the voltage is not maintained through one level.

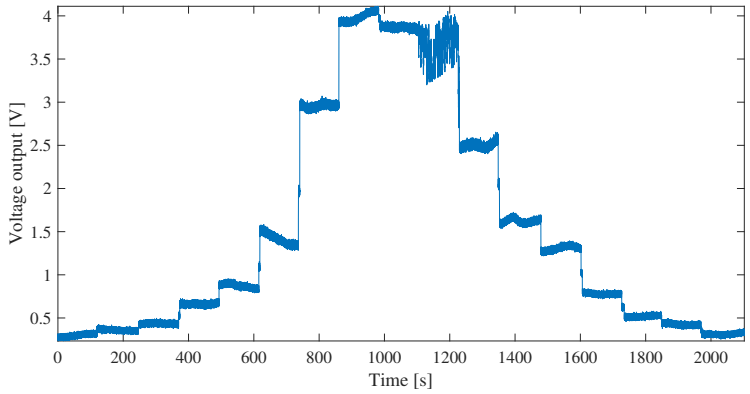

Figure 3.5: Fabry-Perot output sweeping through the DC source with a step in voltage every 10 seconds.

For this reason, the DC source was changed for a wave generator with a ramp signal that could modulate the Fabry-Perot steadily through time and with shorter periods. Moreover, the new modulation method prevented the effect of thermal drifts, since it was much faster.

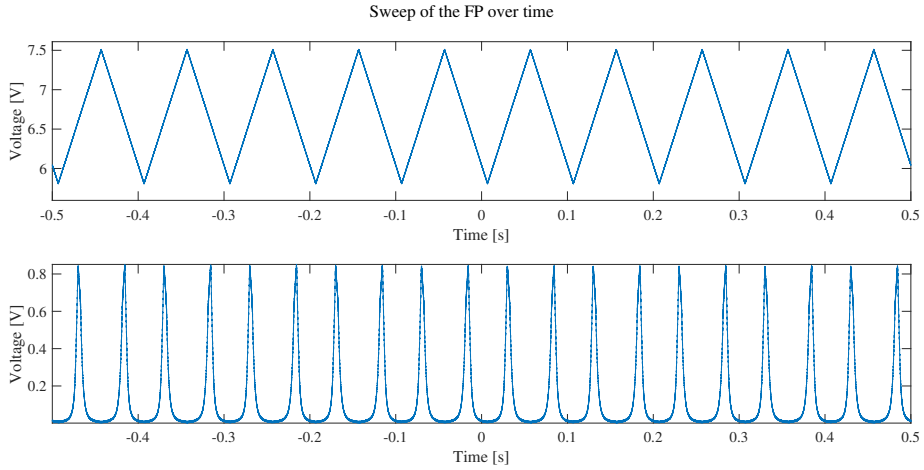

Figure 3.6: Fabry-Perot modulation using a wave generator.

In Figure 3.6, periods of the ramp signal along with the Fabry-Perot output are showed. Unlike with the DC source, the transmission changes are swift and therefore it is considered satisfactory. Moreover, the maximum difference between peaks was 0.01 V, which is considered satisfactory and enables repeatability within experiments as well.

3.2 Experimental measures and analysis

3.2.1 First data

After setting up the configuration, experimental trials were conducted to showcase square wave modulation. The laser diode was modulated at 1 kHz with an am-

plitude of 30 mV and offset of 16 mV, as seen in Figure 3.7 (a). The Fabry-Perot was modulated at 1 Hz between 5.95 and 5.68 V with a symmetric ramp wave. The selection of the Fabry-Perot's period was a compromise, ensuring that the transmission remained relatively stable throughout one cycle of the laser without surpassing the sampling capacity of the oscilloscope and compromising the resolution of the measurements. The sampling frequency of the oscilloscope was 62.5 MHz and the sampling window was 1 second. Therefore, two scans or sweeps of the Fabry-Perot were recorded.

The data treatment and calculations were conducted using Matlab, the complete code can be found in Annex D. The first step consisted on a smoothing of the intensity output, using a moving average with a window size of 100 samples.

An important detail in Figure 3.7 (b) is that individual cycles are asymmetric. This is because when the laser scans in the left side of the Fabry-Perot's peak transmission increases and therefore the intensity output has greater amplitude, whereas in the right side transmission decreases so the intensity through half a period decreases. The contrast between the shapes of the cycles can be appreciated taking a look at Figure 3.7 (c) and (d).

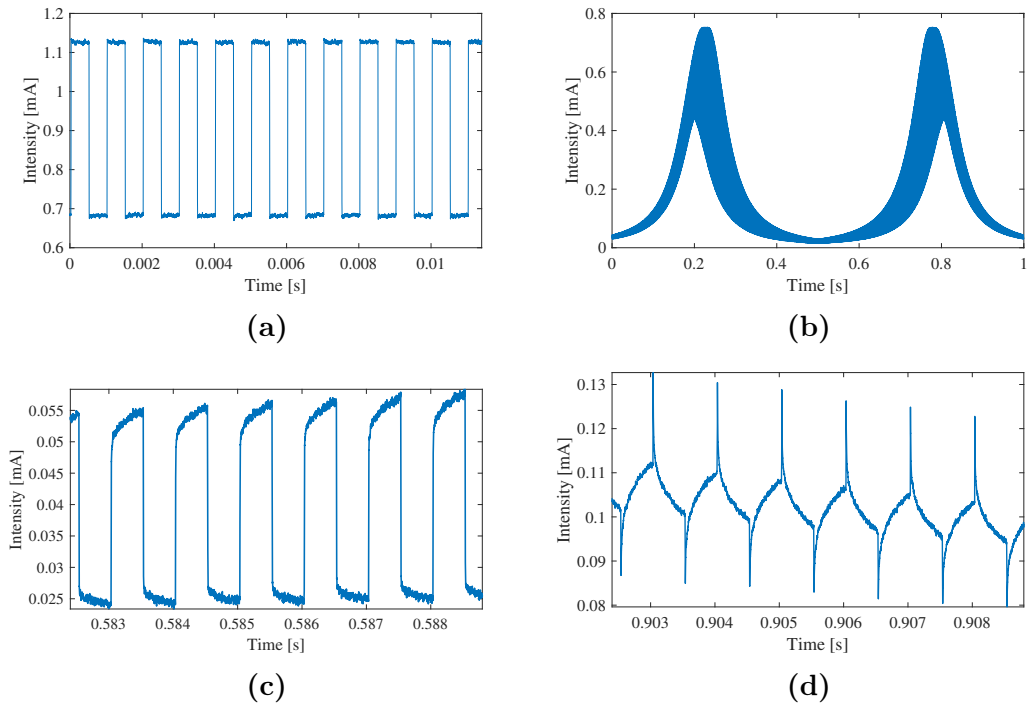

Figure 3.7: **(a)** Zoom on the laser intensity signal. **(b)** A cycle of the transmitted intensity for a full Fabry-Perot modulation. **(c)** Zoom on several cycles on the recorded intensity through the Fabry-Perot on the left side of the peak. **(d)** Zoom on several cycles on the right side of the peak.

Another interesting point is that the two scans of the Fabry-Perot are opposites. The cycles differ in the Fabry-Perot scanning direction, meaning that in the first one mirrors were driven further away while in the second one mirrors were brought closer together.

Transmission function

The initial stage in obtaining results involved extracting the modulation details from the laser's intensity output. The average photocurrent I_0 was 0.668 mA and had an amplitude of 0.387 mA, so the normalized modulation was Δi_m 0.290. Since the sampling was not constant enough to determine a fixed time interval to select the beginning of high and low pulses, the laser intensity was used for this end. The code (Annex D, line 50) detected the end of each pulse in the laser photocurrent and used the same sample number for the transmitted photocurrent, as seen in Figure 3.8. These values dictated the sample pairs used to calculate I_+ and I_- from equation 2.13.

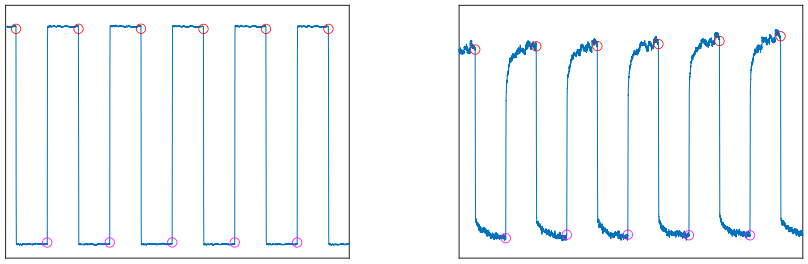

(a) **(b)**

Figure 3.8: **(a)** Pulse detection in the laser diode intensity output. **(b)** The same points in the transmitted intensity samples.

Following this, each pair of samples were added and subtracted to obtain $I+$ and I_- and the results were averaged over every pulse, reducing the effective noise bandwidth to 2 kHz. Since the transmitted intensity for each scan of the Fabry-Perot is asymmetric, I_- also depends on the direction of the scan.

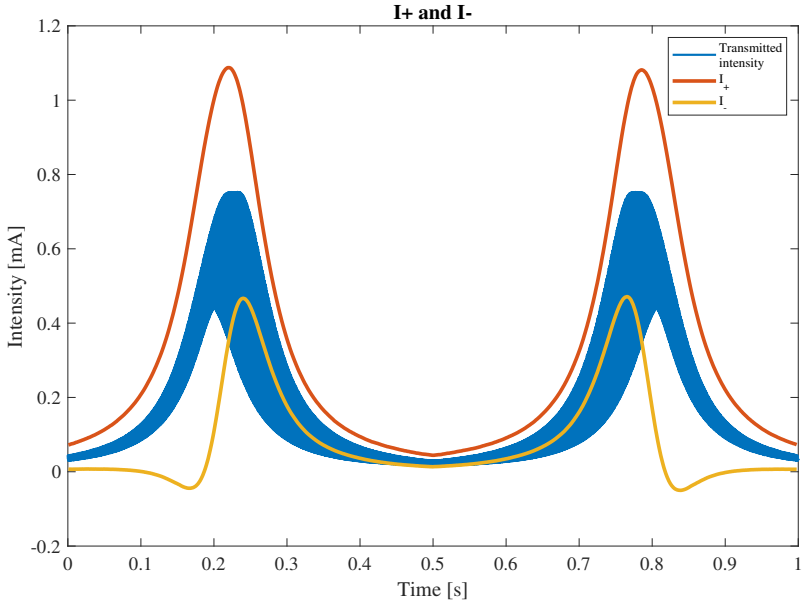

Figure 3.9: Averaged transmission I_{FP}, I_+ and I_- for two Fabry-Perot sweeps.

Using a simple linear conversion, the time axis was adjusted to wavelength following: $\lambda = (t - t_{T/2}) \cdot \frac{\Delta\lambda}{\Delta t}$. So, using the data of one Fabry-Perot sweep, a single transmission spectra could be calculated following equation 2.14. The obtained function had the desired shape and order of magnitude, and therefore validated the method. The full width half maximum recorded with the OSA was 218 pm and the obtained one 210 pm.

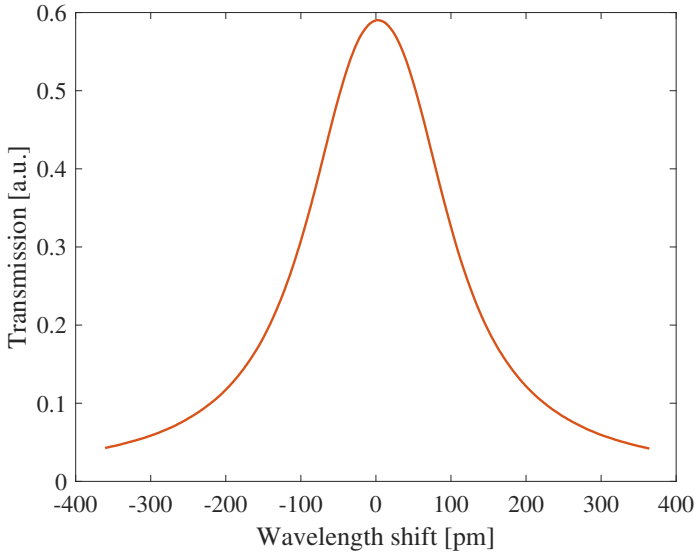

Figure 3.10: Transmission of the Fabry-Perot

Transmission function derivative

There are two ways of calculating the derivative of the transmission function spectra. The first one uses equation 2.14, thus scaling with $\Delta\nu_m < h(t) >$ and was labeled as the "method" derivative. The second one is obtained from directly deriving $\mathscr{L}_0$ and subsequently adapting time to wavelength differential and is referred to as the "calculated" derivative.

To obtain $\Delta\nu_m < h(t) >$ from equation 2.19, the $< \nu > -\nu_0$ values were missing, so shortly after obtaining the intensity data, the spectral output of the laser with and without modulation was measured. The average wavelengths were measured to 1546.92 nm and 1546.89 without and with modulation, respectively. From equation 2.19 it follows that $\Delta\nu_m < h(t) >= 7.10GHz$.

Once this was retrieved, it was possible to calculate both method and calculated derivative, which are both depicted in Figure 3.11. Moreover, the method derivative was scaled to compare the shape, which was considered satisfactory. The order of magnitude had a maximum deviation from the calculated derivative of 30.6%, which is likely linked to the OSA's resolution. The zero crossing, which indicates the position of the peak in the transmission line, was 3.73 pm in the method derivative and 1.77 pm in the calculated one, resulting in a difference between the two approaches of 1.94 pm.

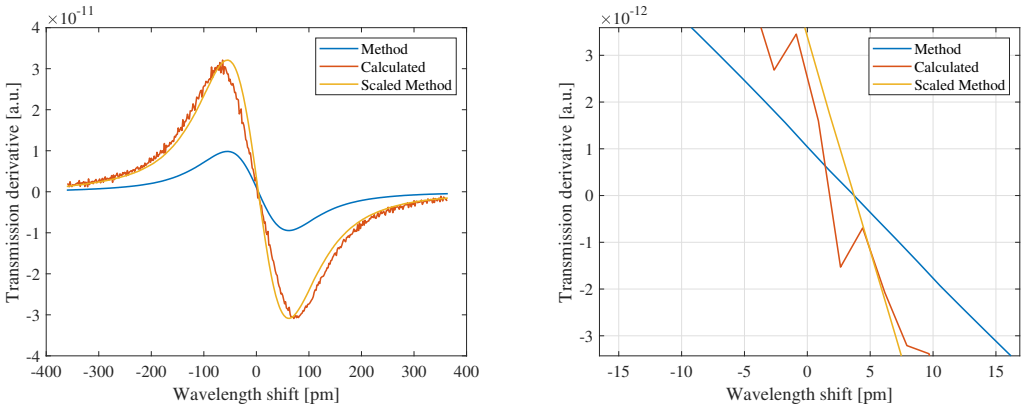

(a) **(b)**

Figure 3.11: **(a)** Transmission derivative comparison. **(b)** Zoom in the zero-crossing of the transmission derivatives.

3.2.2 Noise and resolution

Upon obtaining results, the next step involved evaluating the method's accuracy. To do so, resolution was computed from the calculated noise levels by comparing the curve to a fitted model.

The initial method employed to quantify noise in the transmission spectra and its derivative involved fitting them with Lorentz curves and their respective derivatives. This approach offered the advantage of simplicity in retrieving the initial parameters, facilitating the fitting process. However, it became apparent that the shapes of the transmission and Lorentz curves differed, needing a compromise during the fitting process to accurately adjust the peak or the sides of the line. Upon examining the residuals, it was observed that the main difference came from the omission of second derivative terms, which had been hypothesized in the calculations.

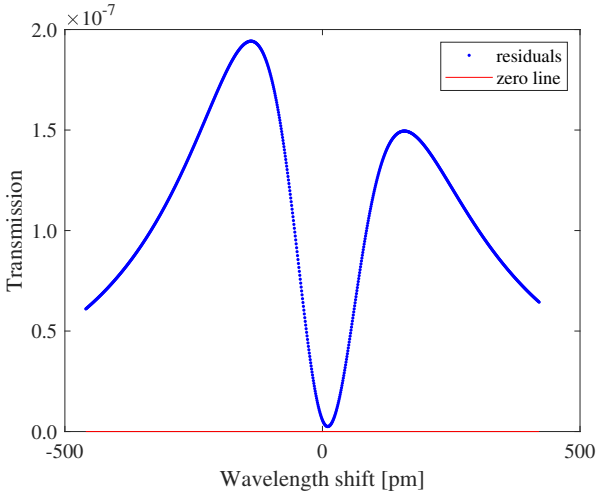

Figure 3.12: Shape of the residuals when fitting the calculated transmission spectra with a Lorentz curve.

Since obtaining a different shape would involve changing the initial calculations completely, another approach for estimating noise was considered. This consisted on dividing the transmission function in sections and adjusting a polynomial to each one from where the standard deviation was calculated.

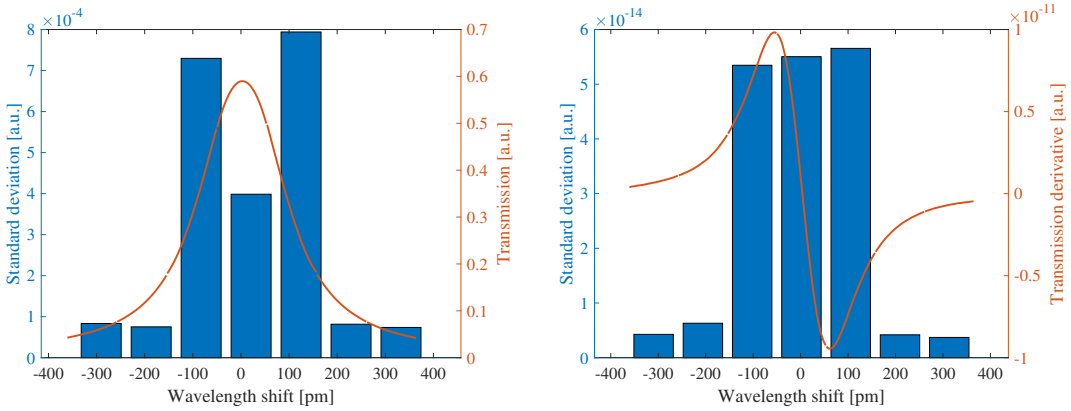

(a) **(b)**

Figure 3.13: **(a)** Sections of the transmission function and their respective standard deviation. **(b)** Sections of the transmission function derivative and their respective standard deviation.

This measurements were still not considered accurate enough, so an alternative approach was considered. This was studying the intensity output only in the transmission peak of the Fabry-Perot. This would be equal to keeping the derivative in the zero crossing and looking at the noise at that point. Results showed that the noise distribution was random (Figure 3.14 (b)) even though a low frequency drift can be observed in the derivative (Figure 3.14 (a)). With an averaging for every half cycle the standard resolution was 1.26 e-14 a.u., which can be translated into a resolution of 0.05 pm.

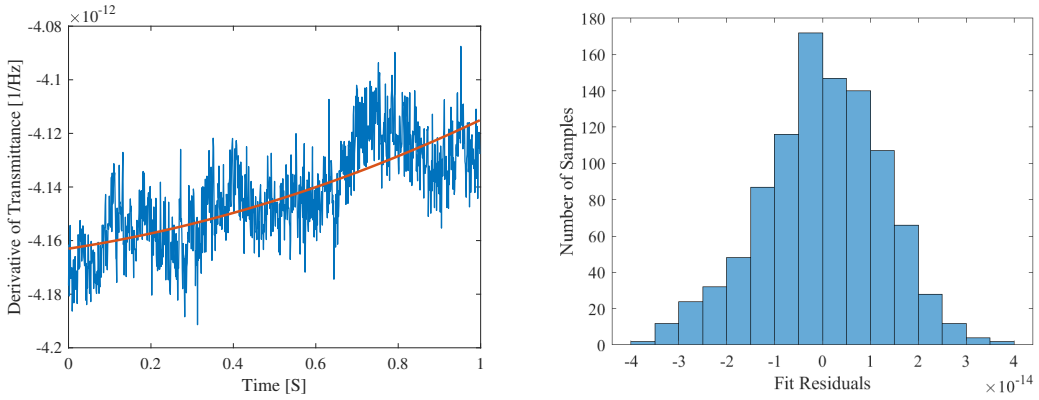

(a) **(b)**

Figure 3.14: **(a)** The derivative and a second order fit of the transmission while the Fabry-Perot is kept at a constant value. **(b)** A histogram of the fit residuals, showing a random and narrow distribution, suggesting the fit removes the drift.

Finally, an evaluation was conducted to determine the impact of averaging on the resolution. Results showed that by averaging 5 samples resolution could be improved by more than 0.01 pm (Figure 3.15) but further averaging was not a significant improvement.

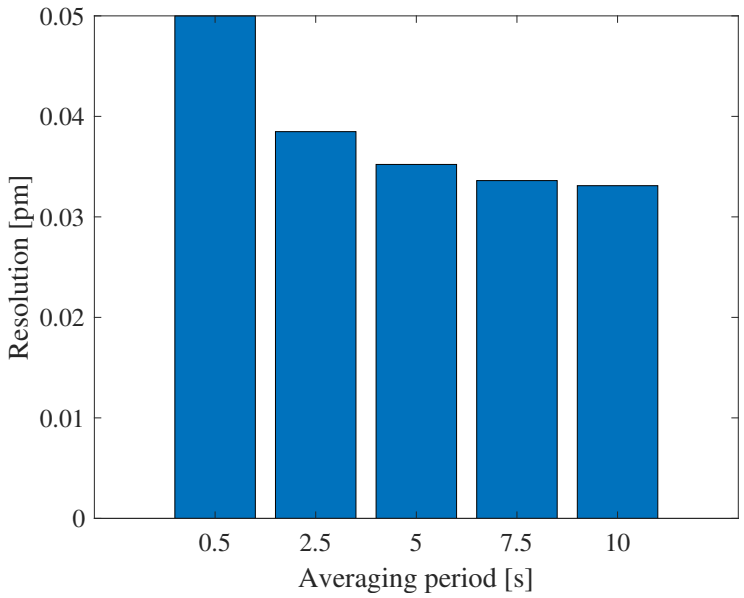

Figure 3.15: Obtained resolution for different averaging samples.

3.2.3 Raw data fitting

A contemplated improvement in the data-treating process was fitting every high and low level of each pulse with a polynomial curve and using these points to calculate I_+ and I_-. The selected number of samples were the same as the ones used in the raw calculation. The aim of this procedure was to reduce the influence of the noise and obtain smoother curves. Moreover, a fit would eliminate the peaks observed in the top of the transmission line, as seen in the figure below.

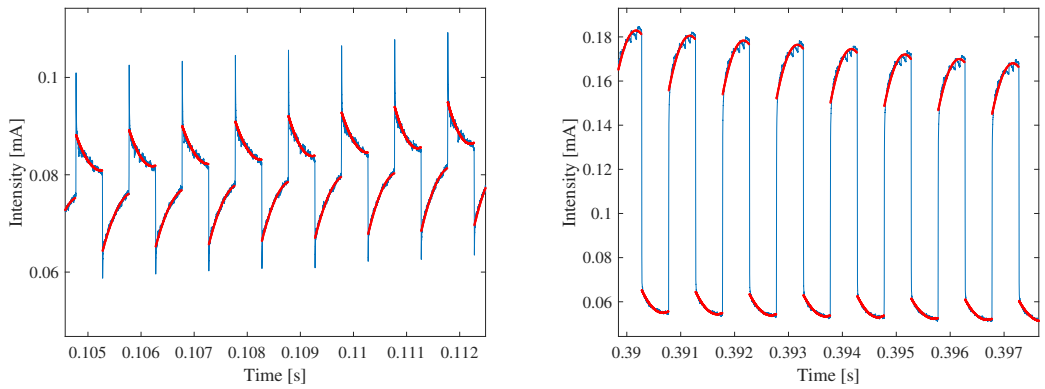

(a) **(b)**

Figure 3.16: **(a)** Fitting in cycles with peaks. **(b)** Fitting in cycles without peaks.

The resulting I_+, I_- and transmission functions were very similar to the ones obtained directly from raw data. The fitting did not show an improvement in resolution either. This was because averaging had a similar effect, making this step unnecessary. Therefore, since the fitting required high computational power and did not give significant improvements it was disregarded for further experiments.

3.2.4 Method robustness

In this section, the influence of Δi_m was tested. The parameter Δi_m quantifies the square wave's modulation and is calculated from the laser's intensity output. It is a key parameter for retrieving the transmission line and derivative, and therefore it needs to be measured adequately. However, in some setups it is not possible to record two intensities simultaneously or split the laser's beam, which makes this measurement susceptible to error. For this reason, the method's sensitivity to Δi_m was assessed.

The study consisted of calculating the transmission and the derivative for $\Delta i_m \pm 0.02$. For the transmission spectra, the first impression was that it did not have the same effects through different wavelength positions, being most influential in the peak where transmission shifted between 0.59 ± 0.0033. In relative terms, a change of 8.1% in Δi_m shifted the transmission peak 0.5% (Figure 3.17).

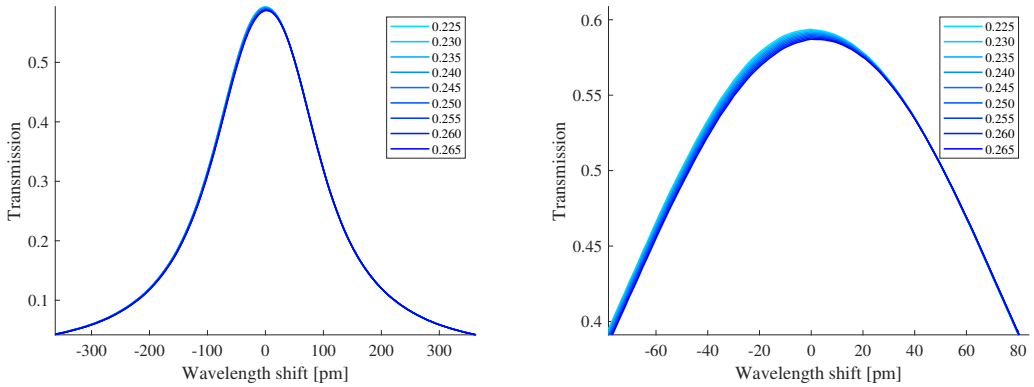

Figure 3.17: **(a)** Transmission spectra for different Δi_m values. **(b)** Zoom in the peak, it is possible to see that the lines are most separated in the top.

The derivative, however, was much more susceptible to changes which affected the local minimum. There, the change was $1.45 \cdot 10^{-12}$, 15.6% of the central value. In the zero crossing, the method's original wavelength shift was 2.01 pm while the variations showed zero crossings in -1.20 pm and 4.42 pm, for the lowest and highest Δi_m, respectively. Therefore, increasing Δi_m shifted the derivative to the left, as depicted in Figure 3.18 (b).

The reason why the change in the derivative is much bigger than in the transmission transmission function can be found in equation 2.14. It can be seen that for the transmission function Δi_m is multiplied by i_-, whereas in the derivative Δi_m

is multiplied by i_+. Since i_+ is much larger than i_-, changes in Δi_m affect the derivative much more than the transmission function.

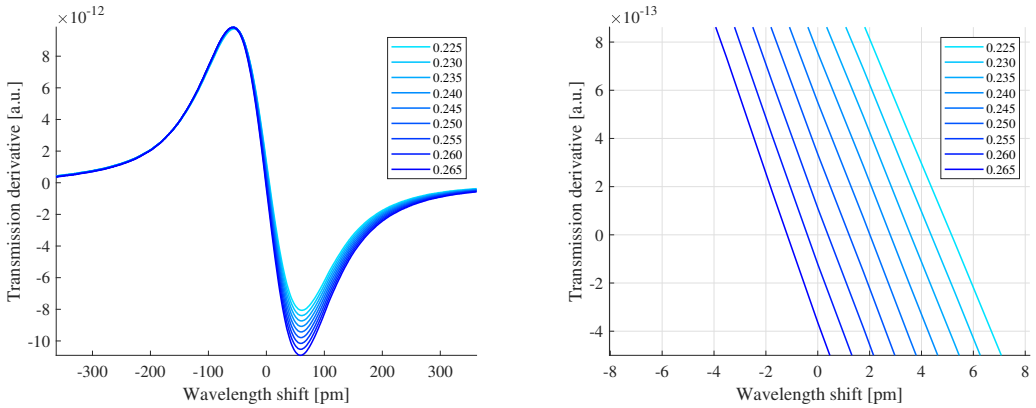

Figure 3.18: **(a)** Transmission spectra derivative for different Δi_m values. **(b)** Zoom in the zero-crossing, where the wavelength shift that gave the peak's position ranged between -1.20 and 4.42 pm.

The expected outcome was that the original value of Δi_m, 0.245, would yield the most symmetric derivative function. However it was seen that the curve with the most similar absolute values of the top and low peak was 0.250. Since Δi_m does not have a tremendous influence on the transmission or on the derivative's zero crossing, it is not a great concern, but it does shed some light on some possible improvements for the setup.

3.2.5 Modulation variations

Once the analysis of the initial data had been completed, another set of experiments was conducted to test the influence of the injection current's intensity modulation amplitude. The aim of these trials was to quantify changes in the transmission spectra and derivative as well as linking the width of the intensity pulse to resolution. Therefore, 5 new data sets were obtained with intensity amplitudes of 22, 24, 26, 28 and 30 mA each.

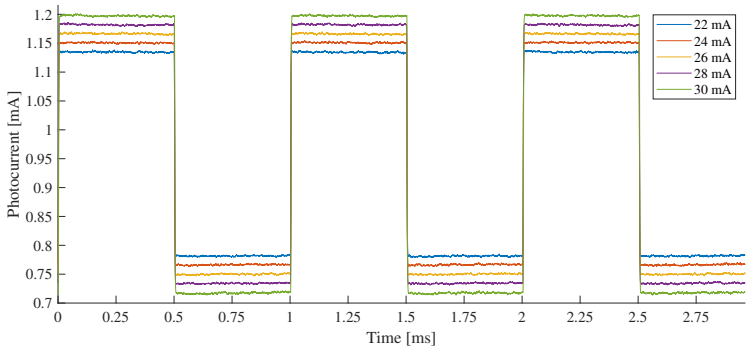

Figure 3.19: Laser's intensity output for the different modulations. A greater injection current yields a greater optical intensity, as expected.

The obtained curves showed that both the transmission and the derivative were affected by the change in modulation. In peaks, the transmission function showed a difference of 5.1% and the derivative 38.5% between the highest and lowest modulation amplitude. The zero crossing was shifted 3.5 pm and the resolution was not significantly changed (Figure 3.20 (c)).

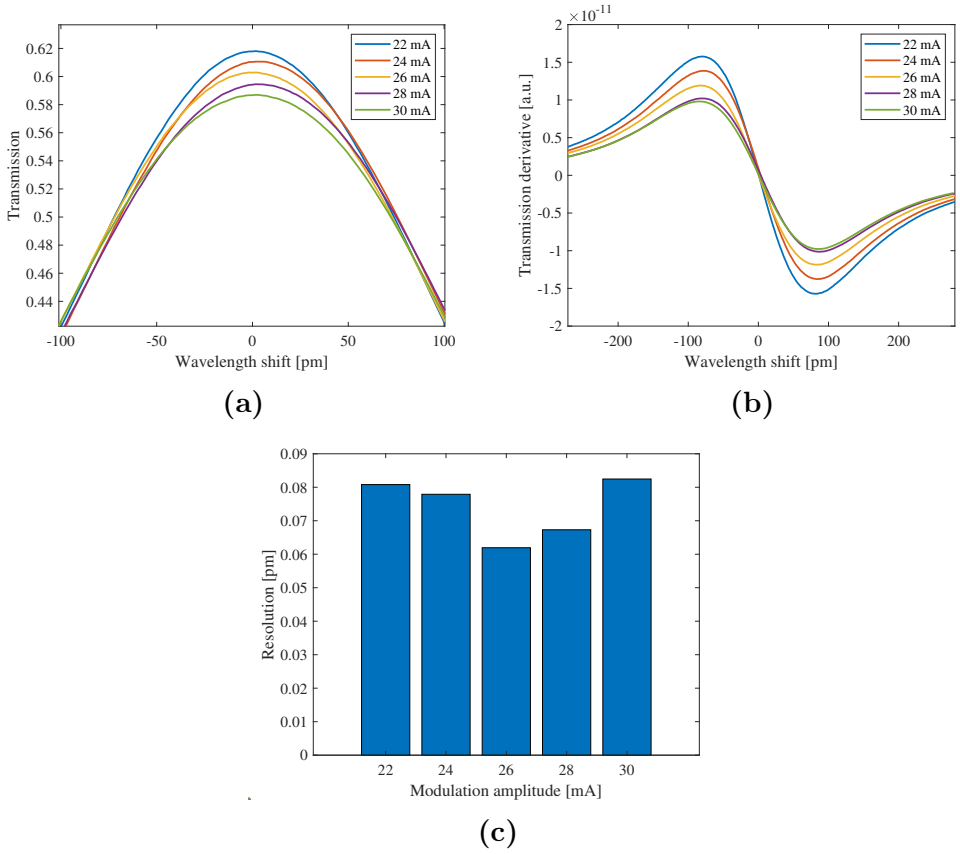

Figure 3.20: **(a)** Zoom in the transmission spectra peak for different laser modulation values. **(b)** Transmission spectra derivative for different laser modulation values. **(c)** Comparison of the resolutions obtained with different modulations.

The divergence in the transmission is considered within the acceptable error range whereas the derivative is not. Moreover, in Figure 3.20 (b) it can be seen that the difference between modulations is not constant. The explanation behind these disparities lies in the optical spectrum analyzer's resolution. Looking back at the calculation for $\mathscr{L}_0'$ (Eq. 2.14) one of the key steps is the scaling with $\Delta\nu_m < h(t) >$, which depends on the average wavelength that is recorded with the OSA. Each modulation amplitude has a different average wavelength which should calibrate $\mathscr{L}_0'$ so measurements are repeatable. The current resolution of the OSA does not yield a reliable measurement of $< \nu >$, therefore, another method for calibrating $\mathscr{L}_0'$ with $\Delta\nu_m < h(t) >$ was attempted.

The principle behind the alternative calibration is to obtain the coefficient $\Delta\nu_m < h(t) >$ from the experimental data. To do so, the maximum values of the curves $\mathscr{L}_0' \cdot \Delta\nu_m < h(t) >$ are normalized by the maximum value of the same curve at a modulation of 22 mA. This yields the coefficient $\frac{\Delta\nu_m <h>}{\Delta\nu_m <h>_{|22}}$ which increases linearly

with modulation.

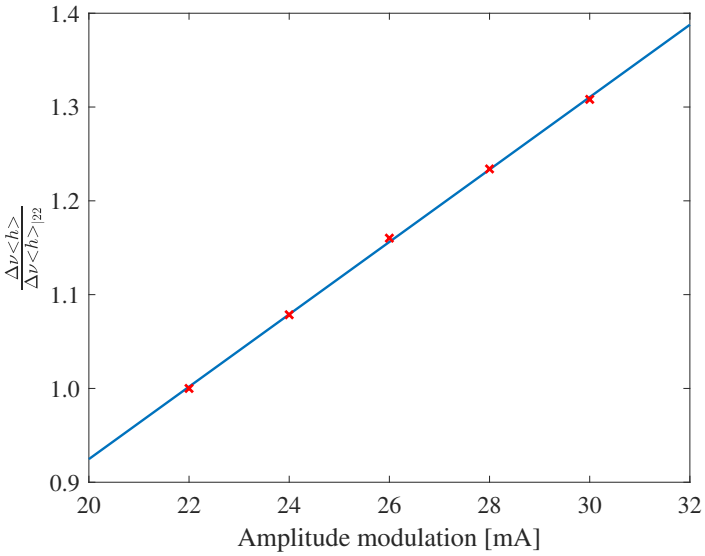

Figure 3.21: Regression of $\frac{\Delta\nu<h>}{\Delta\nu<h>|_{22}}$ and the amplitude of the injection current.

A regression is made from the calculated points, which can be designated as $y = 0.038x + 0.153$ and so each coefficient can be calculated by:

$$\Delta\nu_m < h(t) >_{|i} = \Delta\nu_m < h(t) >_{|22mA} \cdot y_{|i} \tag{3.1}$$

Once the coefficients are retrieved it is possible to obtain $\mathscr{L}_0'$, which was the same for all modulations. Therefore, this method is considered satisfactory and is proposed as a good alternative in case the available OSA is not precise enough.

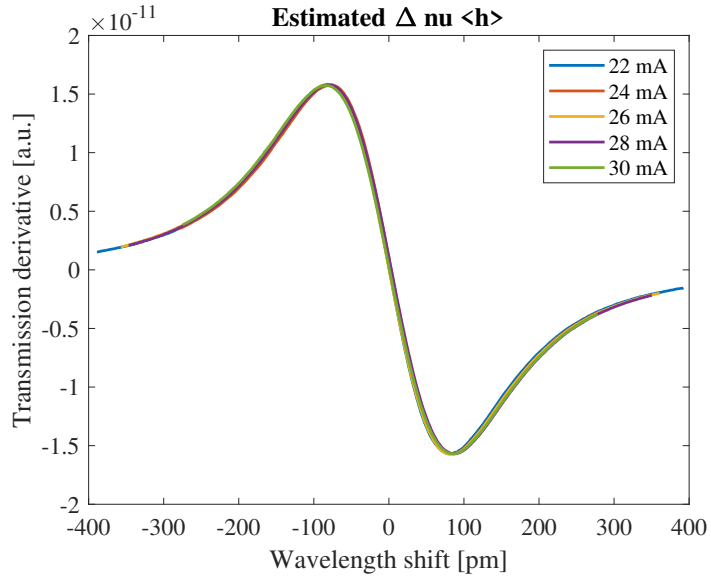

Figure 3.22: Transmission function derivatives for different modulations calibrated experimentally using a regression for $\Delta\nu_m < h(t) >$.

CHAPTER

FOUR

DISCUSSION

This project proved both theoretically and experimentally that square wave modulation is a valid method for interrogating resonant sensors. Using an injection current modulated laser and photodetectors it was possible to retrieve the transmission function and derivative of a Fabry Perot interferometer. After determining the method's noise and resolution, the influence of the amplitude modulation and other parameters was tested to assess the robustness of the system.

Square wave modulation is an alternative to optical interrogation methods such as wavelength modulation spectroscopy and dual wavelength differential detection. With the present approach a resolution of 0.05 pm was achieved, which is 2 to 20 times higher than current high-tech commercial instruments. Moreover, square wave modulation does not require complex calibration procedures such as chirp characterization, phase shift detection for LIA adjustment or RAM characterization. It does not require complex computational operations either.

Because square wave modulation takes advantage of the symmetry in the dynamic chirp, it is only subject to the intensity output and the laser's average frequency with and without modulation. Even though this makes square wave modulation easier to put into practice than other optical methods it also makes it subject to variation in the laser parameters. Depending on the quality of the laser, the parameters that are used to scale the derivative, could change with time. In the most unfavorable cases these measurements would need to be repeated periodically to maintain calibration.

Another issue that came up with the scaling of the derivative was that if the OSA used to probe the laser does not have enough resolution, the method derivative differs noticeably from the calculated derivative. Nevertheless, it was found that the zero crossing was only affected by 1.95 pm and that the shape was still satisfactory.

It was found that the transmission derivative was much more susceptible to changes in the Δi_m coefficient than the transmission function, because it was multiplied by much larger terms. A 8.1% shift in Δi_m changed 0.5% the transmission function peak but 15.6% the derivative.

As for variations in the modulation amplitude, a similar outcome was reached. Transmission was robust to changes whereas the derivative was shifted 38.5%. This was result of the poor resolution of the OSA when measuring the laser's average wavelength. This set of tests was used to prove an alternative calibration approach. By dividing the maximum values of the unscaled derivatives and making a regression with the modulation values it was possible to obtain $< h > \Delta\nu_m$ experimentally.

One further aspect to consider is the noise in the set up. Even though the achieved resolution is satisfactory, the setup has to be optimized in several aspects such as reducing mechanical vibrations and optical interference. However, thanks to averaging every cycle noise was reduced to an effective bandwidth of 2 kHz. This could even be reduced by optimizing data acquisition. The oscilloscope that was used to measure the photocurrents had a maximum sampling frequency of 62.5 MHz over one second. Signal recovery with LabView could improve sampling capacity and overall noise reduction.

Noise levels were assessed using polynomial fits and the standard deviation in the residuals. Even though a Fabry-Perot transmission function can be assimilated with a Lorentzian curve, it was found that the residuals in the fitting were shaped like the second derivative of the function. This was because initial hypothesis ignored the influence of the second derivative, in further research projects calculations could be modified to include it.

The practical implication of square wave modulation is that a high-precision and robust optical interrogation technique is now more practical and much cheaper than other optical alternatives. Therefore, it is more accessible to researchers as well as industry. Moreover, the application could be tested with other kinds of sensors such as fiber Bragg gratings and their practical applications.

CHAPTER

FIVE

CONCLUSIONS

The results and analysis presented in this project prove square wave modulation as a high-precision yet cost effective simplified optical interrogation technique. The suggested approach is able to retrieve the transmission function and derivative of a resonant optical sensor from a measurement of a photocurrent through time and potentially with only one characterization of the laser's average wavelength. The obtained resolutions is 0.05 pm, using only simple instrumentation such as an injection modulated laser, wave generator and photodiodes.

The technique could be improved the following ways:

- Rethink initial calculations to include the second derivative and grant a better fit of the transmission function.
- Improve data acquisition in the setup to increase the averaging capacity and thus reduce the effective noise bandwidth.

Aside from this improvements, this simplified optical interrogation can also be tested with other interferometers like fiber Bragg gratings, which offer a wide range of sensing solutions.

To sum it all up, square wave modulation is a promising new approach to optical interrogation. The consolidation of this method brings together optical superior sensing performance with versatile, practical and low cost electronic solutions.

REFERENCES

[1] F. Kapron, D. B. Keck, and R. D. Maurer, "Radiation losses in glass optical waveguides," *Applied Physics Letters*, vol. 17, no. 10, pp. 423–425, 1970.

[2] H. Ishikawa, "Introduction," in *Ultrafast All-Optical Signal Processing Devices*. John Wiley & Sons, 2008, ch. 1, pp. 1–14, ISBN: 9780470758694.

[3] R. Narayanaswamy and O. S. Wolfbeis, "Optical technology until the year 2000: An historical overview," *Optical Sensors: Industrial Environmental and Diagnostic Applications*, pp. 1–34, 2004.

[4] J. D. Montgomery, "Chapter 1 - history of fiber optics," in *Fiber Optic Data Communication*, C. DeCUSATIS, Ed., San Diego: Academic Press, 2002, pp. 3–31, ISBN: 9780122078927.

[5] E. Udd *et al.*, "Fiber optic distributed sensing systems for harsh aerospace environments," in *Smart Structures and Materials 1999: Industrial and Commercial Applications of Smart Structures Technologies*, J. H. Jacobs, Ed., International Society for Optics and Photonics, vol. 3674, SPIE, 1999, pp. 136–147, ISBN: 9780819431486.

[6] A. Méndez and A. Csipkes, "Overview of fiber optic sensors for ndt applications," in *Nondestructive Testing of Materials and Structures*, O. Güneş and Y. Akkaya, Eds., Dordrecht: Springer Netherlands, 2013, pp. 179–184, ISBN: 9789400707238.

[7] P. Roriz, L. Carvalho, O. Frazão, J. L. Santos, and J. A. Simões, "From conventional sensors to fibre optic sensors for strain and force measurements in biomechanics applications: A review," *Journal of Biomechanics*, vol. 47, no. 6, pp. 1251–1261, 2014.

[8] J. L. Cano Perez *et al.*, "Fiber optic sensors: A review for glucose measurement," *Biosensors*, vol. 11, no. 3, 2021.

[9] X.-d. Wang and O. S. Wolfbeis, "Fiber-optic chemical sensors and biosensors (2015–2019)," *Analytical Chemistry*, vol. 92, no. 1, pp. 397–430, 2019.

[10] T. He, F. Wen, Y. Yang, X. Le, W. Liu, and C. Lee, "Emerging wearable chemical sensors enabling advanced integrated systems toward personalized and preventive medicine," *Analytical Chemistry*, vol. 95, no. 1, pp. 490–514, 2023.

[11] E. Udd, "An overview of fiber-optic sensors," *Review of Scientific Instruments*, vol. 66, no. 8, pp. 4015–4030, 1995.

[12] P. Hariharan, *Basics of interferometry*. Elsevier, 2010, ISBN: 9780080918617.

[13] M. Bass, E. W. Van Stryland, D. R. Williams, and W. L. Wolfe, *Handbook of optics*. McGraw-Hill New York, 1995, vol. 2, ISBN: 9783527606689.

[14] G. L. Mitchell, "Intensity-based and fabry–perot interferometer sensors," *Fiber optic sensors: an introduction for engineers and scientists*, pp. 119–134, 2011.

[15] B. Saleh and M. C. Teich, *Fundamentals of Photonics*. John Wiley & Sons, 2019, ISBN: 9780471358329.

[16] J. M. Supplee, E. A. Whittaker, and W. Lenth, "Theoretical description of frequency modulation and wavelength modulation spectroscopy," *Applied Optics*, vol. 33, no. 27, pp. 6294–6302, 1994.

[17] P. Kluczynski, J. Gustafsson, Å. M. Lindberg, and O. Axner, "Wavelength modulation absorption spectrometry—an extensive scrutiny of the generation of signals," *Spectrochimica Acta Part B: Atomic Spectroscopy*, vol. 56, no. 8, pp. 1277–1354, 2001.

[18] P. Pokrowsky, W. Zapka, F. Chu, and G. Bjorklund, "High frequency wavelength modulation spectroscopy with diode lasers," *Optics communications*, vol. 44, no. 3, pp. 175–179, 1983.

[19] G. B. Rieker, J. B. Jeffries, and R. K. Hanson, "Calibration-free wavelength-modulation spectroscopy for measurements of gas temperature and concentration in harsh environments," *Appl. Opt.*, vol. 48, no. 29, pp. 5546–5560, Oct. 2009.

[20] J. E. Duque, M. Jaramillo, S. López, P. Torres, and A. Molina, "Real-time, in situ measurement of h 2 o generated during in situ combustion tests using 1f-normalized wavelength modulation spectroscopy with second harmonic detection," *Applied Optics*, vol. 62, no. 1, pp. 108–116, 2023.

[21] J. Li *et al.*, "Simultaneous standoff sensing for methane and hydrogen sulfide using wavelength-modulated laser absorption spectroscopy with non-cooperative target," *Sensors and Actuators B: Chemical*, vol. 374, p. 132 825, 2023.

[22] N. Liu, L. Xu, and J. Li, "Self-calibrated wavelength modulation spectroscopy based on 2 f/1 f amplitude and integral area for trace gas sensing," *Optical and Quantum Electronics*, vol. 55, no. 1, p. 22, 2023.

[23] J. Wang *et al.*, "Microbiological total viable count detection based on tunable diode laser wavelength-modulation spectroscopy," *Sensors and Actuators B: Chemical*, p. 133 332, 2023.

[24] IUPAC, *IUPAC Goldbook -Beer–Lambert law*, Last accessed 3rd March 2023. [Online]. Available: `https://goldbook.iupac.org/terms/view/B00626`.

[25] E. Moses and C. Tang, "High-sensitivity laser wavelength-modulation spectroscopy," *Optics letters*, vol. 1, no. 4, pp. 115–117, 1977.

[26] M. Kwaśny and A. Bombalska, "Optical methods of methane detection," *Sensors*, vol. 23, no. 5, p. 2834, 2023.

[27] A. Behera and A. Wang, "Calibration-free wavelength modulation spectroscopy: Symmetry approach and residual amplitude modulation normalization," *Applied optics*, vol. 55, no. 16, pp. 4446–4455, 2016.

[28] K. Duffin, "Wavelength modulation spectroscopy with tunable diode lasers, a calibration-free approach to the recovery of absolute gas absorption lineshapes," Ph.D. dissertation, Strathclyde university, 2007.

[29] F. Ouellette, J. Li, Z. Ou, and J. Albert, "High-resolution interrogation of tilted fiber bragg gratings using an extended range dual wavelength differential detection," *Optics Express*, vol. 28, no. 10, pp. 14 662–14 676, 2020.

[30] G. Stewart, W. Johnstone, J. R. Bain, K. Ruxton, and K. Duffin, "Recovery of absolute gas absorption line shapes using tunable diode laser spectroscopy with wavelength modulation—part i: Theoretical analysis," *Journal of Lightwave Technology*, vol. 29, no. 6, pp. 811–821, 2011.

[31] K. Duffin, A. J. McGettrick, W. Johnstone, G. Stewart, and D. G. Moodie, "Tunable diode-laser spectroscopy with wavelength modulation: A calibration-free approach to the recovery of absolute gas absorption line shapes," *Journal of Lightwave Technology*, vol. 25, no. 10, pp. 3114–3125, 2007.

[32] C. S. Goldenstein, C. L. Strand, I. A. Schultz, K. Sun, J. B. Jeffries, and R. K. Hanson, "Fitting of calibration-free scanned-wavelength-modulation spectroscopy spectra for determination of gas properties and absorption lineshapes," *Applied optics*, vol. 53, no. 3, pp. 356–367, 2014.

[33] M. Csele, *Fundamentals of light sources and lasers*. John Wiley & Sons, 2011, ISBN: 9780471675228.

[34] L. Garwin and T. Lincoln, *A century of nature: twenty-one discoveries that changed science and the world*. 2010, ISBN: 9780226284163.

[35] H. J. Eichler, J. Eichler, and O. Lux, *Lasers - Basics, Advances and Applications*. Springer International Publishing, Nov. 2018, vol. 220, pp. i–xi/1-511, ISBN: 9783319998954.

[36] G. Morthier and P. Vankwikelberge, *Handbook of distributed feedback laser diodes*. Artech House, 2013, ISBN: 9781608077014.

[37] S. Miller, T. Li, and E. Marcatili, "Part ii: Devices and systems considerations," *Proceedings of the IEEE*, vol. 61, no. 12, pp. 1726–1751, 1973.

[38] Thorlabs, *Broadband sources*, Last accessed 2nd March 2023. [Online]. Available: `https://www.thorlabs.com/newgrouppage9.cfm?objectgroup_id=4285`.

[39] J. A. Buck, *Fundamentals of optical fibers*. John Wiley & Sons, 2004, vol. 50, ISBN: 9780471221913.

[40] Thorlabs, *Laser specifications*, Last accessed 2nd March 2023. [Online]. Available: `https://www.thorlabs.com/newgrouppage9.cfm?objectgroup_id=1297&pn=DET01CFC`.

[41] Vigneshdm1990, *CC BY-SA 4.0*, Last accessed 2nd March 2023. [Online]. Available: `https://commons.wikimedia.org/w/index.php?curid=87147564`.

APPENDICES

A - DETAILED DESCRIPTION OF OPTICAL COMPONENTS

A1- Optical light sources

Optical sources are essential components in optical sensing systems as they provide the necessary light for the system to operate. There exists a wide range of light sources, and choosing one depends on the specific application and the required characteristics of the light. Depending on the source, the energy required to activate the material and emit light can be in the form of heat, chemical, or electrical energy [13].

Semiconductor materials are commonly used as light sources in optical sensing systems. To emit light, the semiconductor material is excited by a voltage field across the n and p regions, resulting in an excess of holes and electrons and bringing the material to an excited state. The holes and electrons then recombine, returning to a minimal energy level in one of two ways: radiatively or non-radiatively. In radiative recombination, a photon is emitted, creating light in a time period known as τ_r. In non-radiative recombination, the material dissipates energy as heat in a time period known as τ_n.

The efficiency of a semiconductor-based light source depends on the ratio between the time constants of the two types of emissions, which in turn depends on factors such as impurities, electrically induced damage centers, and heating. A small τ_r/τ_n ratio results in a more efficient light source, as it indicates that more energy is being dissipated through radiative emission. The overall efficiency of the light source is typically designated using the following formula.

$$\eta = \frac{1}{1 + \tau_r/\tau_n} \tag{1}$$

Optical materials such as GaAs, GaAlAs, InGaAsP, and InP are commonly used in light sources, with radiative lifetimes τ_r typically in the range of 10^{-8} to 10^{-10} seconds [33]. These materials possess a direct bandgap, meaning that a single photon can excite a single electron to jump across the bandgap.

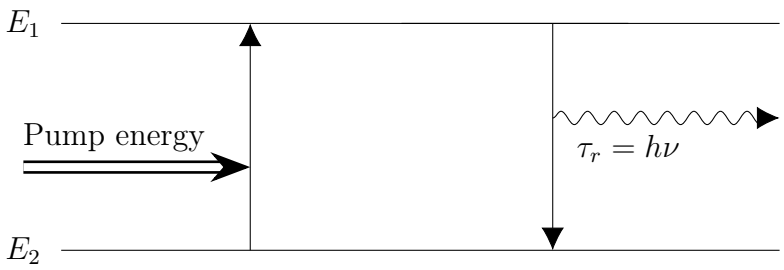

Figure A.1: Energy transfer in a light emitting semiconductor.

Once the material is excited, it can undergo one of three types of emissions based on photon interactions: spontaneous emission, stimulated emission, or superradiance. In spontaneous emission, each photon is released independently and the probability of interaction between states is low. As a result, this type of emission produces a wide spectral linewidth due to the different emission energies of each photon. The shape of the linewidth is affected by quantum mechanics, pressure, and temperature of the semiconductor. Optical sources using spontaneous emission have low noise, are immune to optical feedback, and are highly reliable.

On the other hand in stimulated emission when the photon flux is high enough, there is a high probability that it will stimulate an excited state to radiate as well. The triggered photon will have the same wavelength and phase as the old one. Therefore, stimulated emission creates coherent light beams. While the probability of a photon releasing another photon is higher than one, the semiconductor will increase its output intensity to try to reach an equilibrium to compensate the population inversion state.

If a stimulated emission light source has to operate in a continuous mode, the input power must be balanced with the absorption and release probabilities. In other words, there has to be a generation or stimulation of a photon for each one lost in absorption.

Coherent light sources are activated through spontaneous emission, which triggers stimulated emissions in a condition called the threshold. When it mainly runs on stimulated emission and there is a feedback, the source is said to be lasing.

Finally, superradiance is an intermediate between spontaneous and stimulated emission. There is a high level of spontaneous emission that triggers stimulated emission, but there is no recirculation, leading to low coherence in the source.

Knowing these characteristics, we can list the parameters that are relevant when choosing a light source.

1. **Spectral output:** The range of wavelengths that it can emit, different sensors require different spectral regions.

2. **Power:** It determines the intensity of the beam. This requirement depends on the tested sample (size and optical properties) as well as the sensor (working range).

3. **Stability:** It refers to how long can the source provide a continuous and unchanged beam. Depending on the nature of the measurement, the provided light needs to be reliable during different intervals of time.

4. **Coherence:** The ability of the source to generate waves with the same phase. It is measured as a length parameter. Some sensors such as interferometers use phase measurements to gather information, if coherence is lost the measurement is incorrect.

Lasers

A laser (acronym for Light Amplification by Stimulated Emission of Radiation) is a type of light source that runs on stimulated emission. To do so, it uses a photon flux above the threshold condition, which creates a light beam that is highly coherent and has a narrow spectral band. The spectral gain of the semiconductor can be wider but a recirculation within the laser limits its bandwidth.

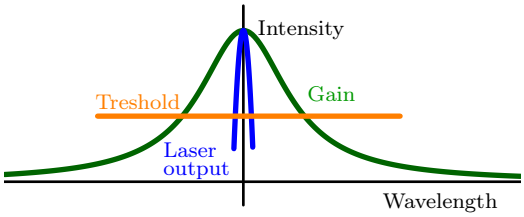

Figure A.2: Energy transfer in a light emitting semiconductor and a laser.

It is essentially an optical oscillator made up of two main components that act as an amplifier and a positive feedback: an active medium and a resonant cavity. These two elements are connected with matching phase and so when the active medium starts emitting photons, they will be amplified in the resonant cavity and fed into the active medium again to create a stronger beam. The cycle will go on until the output power is strong enough. At this point, the amplifier gain will decrease to match the system losses and then the laser will have reached a steady state.

Although the laser working principle was theoretically described by Einstein as early as 1917, the first ruby laser was not created until 1960 by Theodore H. Maiman [34]. Since then, other types of active mediums have been discovered, including gas, chemical, and solid-state materials [35].

For the specific application described in this project, a laser diode with distributed feedback was used. The active region of a DFB laser contains a diffraction grating that provides wavelength selection optical feedback, resulting in continuous reflection along the cavity. This makes the laser more stable and yields extremely narrow line widths [36].

Lasers can function in continuous or pulsed waves, depending on their power

output through time. Continuous lasers need a steady source of photons to have a constant population inversion whereas pulsed lasers operate discontinuously at a fixed repetition rate. The three main ways of obtaining pulsed signals are Q-switching, mode-locking and pulsed pumping.

As well as changing their intensity through time, some lasers can be modulated in wavelength. A laser chirp is known as the change of frequency over time of a laser pulse. Laser chirp can be used to extract information from sensing applications, similarly to spectroscopy.

When taking measures with a laser it's important to take into account that the typical laser spectrum also has some side modes that can influence the sensing measurements. There are different phenomena that can induce mode hopping, like temperature and intensity changes as well as optical feedback from the sensing system. Even though some lasers can include elements to prevent these variations, several components can be added to the optical system too. They are discussed in section A4.

White light source

As opposed to lasers, white light sources emit within a broad optical bandwidth and have low coherence. This is achieved with the use of superluminescent diodes. These semiconductors provide the high power of lasers combined with the low coherence of diodes [37]. The optical output is amplified, but does not have the feedback needed to provide coherent light, resulting in excellent high power broadband light with low speckle noise [38].

The application of white light sources in this project has been focused on the characterization of interferometers and providing a reliable source for equipment checks.

A2- Optical fibers

An optical fiber is a flexible filament with a circular section made up of glass or plastic capable of transmitting light. It is made up of a transparent core covered by a cladding and both are protected by an outer plastic coating. The core and cladding have different refractive indexes, when a light beam goes into the cladding at an angle greater than the critical angle it undergoes total internal reflection and it bounces off without suffering any losses from absorption or scattering [39].

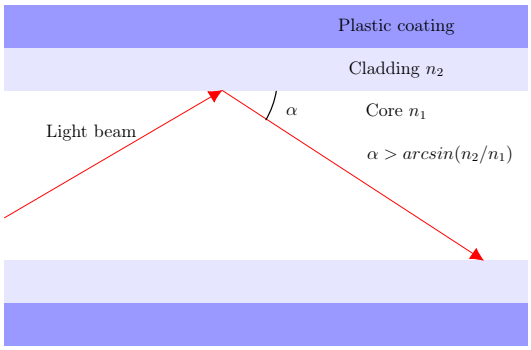

Figure A.3: Energy transfer in a light emitting semiconductor and a laser.

Light propagates inside a fiber in different modes. Since every mode will travel at a different velocity through the fiber there is a limited amount of waves that can be sent through the fiber without overlapping one pulse with the next one. This phenomenon is called modal dispersion. Fibers that have a small core diameter are named single-mode fiber and only allow one type of mode through. Multimode fibers allow more than one mode through them and some of them might have a graded reflective index to mitigate modal dispersion.

Optical fiber was the key invention for making light communication and sensing possible since it provided the necessary transmission medium. They have low losses over long distances, are flexible, lightweight and small, along many other benefits mentioned in section 2.1. All the described optical components in the setup are connected through optical fibers.

A3- Photodetectors

When choosing a photodetector, several figures of merit must be taken into account. Thorlabs, a manufacturer of optical instruments includes the following ones [40].

- **Quantum efficiency:** The probability that a photon will generate a carrier that contributes to the output current. To compute it, the total flux of electrons is divided by the incident photon flux. The mechanisms that hinder the photoelectric effect are different for every material. They are reflectivity of the photodetector surface, photons that avoid recombination and electrons that are absorbed by the material. These phenomena explain why quantum efficiency is wavelength dependant which is why every material has an optimal wavelength window.

- **Responsivity:** The relationship between the electrical input and optical output power. Responsivity is directly proportional to quantum efficiency and free-space wavelength. It limits the optical system's power since the detector can saturate at high powers. Additionally, responsivity determines the dynamic range of the sensor.

- **Response time:** The speed at which free carriers leave the semiconductor is known as the response time. It is calculated as the time it takes to go from 10% to 90% of the total final output.

- **Dark current:** When photodetectors do not have any optical inputs they can discharge electrical currents that are known as dark currents. These electron-hole pairs are generated thermally or through tunneling and are completely random. Every 10°C increase in temperature the dark current doubles.

The operating characteristics of photodiodes are influenced by the operating mode, which is determined by the voltage applied to the semiconductor. There are two primary modes of operation: photoconductive and photovoltaic. In the photoconductive mode, a reverse bias is applied, which widens the p-n junction and increases the detector's responsivity while reducing its capacitance. This mode offers faster response times but also produces higher levels of dark current. Additionally, the detector's gain is dependent on the bias voltage and is sensitive to changes in temperature. The photoconductive mode is commonly used in small optical systems that require high-speed detection. Photovoltaic mode is when the bias is null and the voltage builds up in the photodetector. This will create a sensor with minimal dark currents but it will also have lower responsivity.

A4- Other components

Isolator or circulator

An optical isolator is a device that prevents reflected light from returning back to the source by transmitting in one way only [15]. Isolators, also known as circulators, act as a one way valve and prevent harmful effects on the lasers. These kind of devices are known as nonreciprocal polarization devices since their working principle is based on a Faraday rotator between two polarizers oriented with a 45°shift. The Faraday rotator is a reciprocal polarization device, which means that its effect is the same for beams going in opposite ways.

When the incident beam enters the first polarizer it is set at 0°, then it is rotated 45°, following the rule of the right hand, then it can pass through the second polarizer without losing intensity. However, a reflected ray will go the other way, it enters the faraday rotator with an angle of 45°and it will exit it at an orientation of 90°. Since it is orthogonal to the first polarizer it will be completely blocked. Since Fabry-Perots reflect a portion of the light that goes through them it is important to use a circulator to prevent laser damage and interferences in the setup.

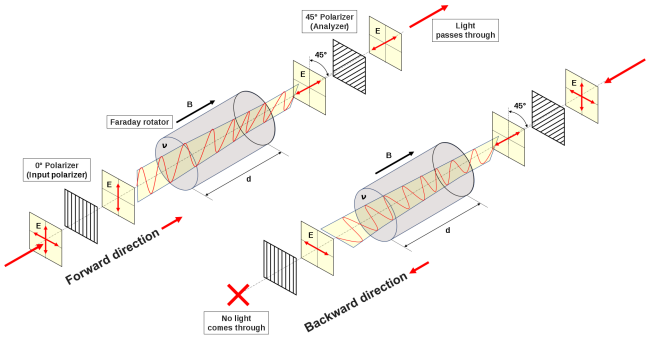

Figure A.4: Working principle of an isolator. Figure taken from [41], used under Creative Commons CC-BY-SA 4.0.

Attenuator

An optical attenuator is a device used to limit the magnitude of the power level of an optical signal. Attenuation is associated with different kind of losses and so it can be achieved through absorption, reflection, diffusion, scattering, etc. Typically, attenuators have an operation wavelength range in which they can maintain equal losses and need to be selected accordingly to the source's wavelength window. Optical attenuators are used to prevent the overload of sensible equipment or match the sensitivity of the sensing equipment, like preventing photodetector saturation.

A useful mechanism when attenuators are not available is coiling the optical fibers in a short radius. The coiling will lead the light into the cladding which will introduce some absorption losses in the system.

Temperature controller

As mentioned before, the Fabry-Perot is sensible to temperature changes, therefore a temperature controller that ensures its stability. The device works with a PID controller that can be adjusted to the setup.

B - SQUARE WAVE WMS DERIVATION

B1 - Isolation of the Lorentz lineshapes

The initial equations expressed the intensities I_+ and I_- as:

$$\begin{aligned} I_+ &= I_{FP} + I_{FP}(ts + T/2) = 2[I_0\mathscr{L}_0 + \Delta I_m \Delta\nu_m \mathscr{L}_0' h(t_s)] \\ I_- &= I_{FP} - I_{FP}(ts + T/2) = 2[\Delta I_m \mathscr{L}_0 + I_0 \mathscr{L}_0' \Delta\nu_m h(t_s)] \end{aligned} \tag{2}$$

I_+ and I_- can be expressed as a matrix equation.

$$\begin{pmatrix} I_+ \\ I_- \end{pmatrix} = 2 \begin{pmatrix} I_0 & \Delta I_m \\ \Delta I_m & I_0 \end{pmatrix} \begin{pmatrix} \mathscr{L}_0 \\ \mathscr{L}_0' \Delta\nu_m h(t_s) \end{pmatrix} \tag{3}$$

Which can be assimilated as:

$$A = 2B \cdot C$$

The inverse of the intensity term is:

$$B^{-1} = \frac{1}{I_0^2 - \Delta I_m^2} \begin{pmatrix} I_0 & -\Delta I_m \\ -\Delta I_m & I_0 \end{pmatrix} \tag{4}$$

Finally the isolated transmission lines are:

$$\begin{aligned} \begin{pmatrix} \mathscr{L}_0 \\ \mathscr{L}_0' \Delta\nu_m h(t_s) \end{pmatrix} = \frac{1}{2I_0} \cdot \frac{1}{1 - (\Delta I_m / I_0)^2} \begin{pmatrix} 1 & \frac{-\Delta I_m}{I_0} \\ \frac{-\Delta I_m}{I_0} & 1 \end{pmatrix} \begin{pmatrix} I_+ \\ I_- \end{pmatrix} = \\ = \frac{1}{2(1 - \Delta i_m^2)} \begin{pmatrix} 1 & -\Delta i_m \\ -\Delta i_m & 1 \end{pmatrix} \begin{pmatrix} i_+ \\ i_- \end{pmatrix} \end{aligned} \tag{5}$$

B2 - Average frequency calculation

The contribution to a unique frequency for each modulation level is expressed by the following equation:

$$< \nu_{\pm} >= \frac{[\frac{T}{2}\nu_0 \pm \frac{T}{2}\Delta\nu_m < h(t) >] \cdot [P_0 \pm \Delta P]}{\int S(\nu)d\nu} \tag{6}$$

Which is obtained by the following procedure:

$$\begin{aligned} < \nu_{\pm} >= \frac{\int \nu P_{\pm}\frac{dt}{d\nu}d\nu}{\int S(\nu)d\nu} = \frac{\int \nu P_{\pm}dt}{\int S(\nu)d\nu} = \\ = \frac{\int_0^{T/2}[\nu_0 \pm \Delta\nu_m h(t)][P_0 \pm \Delta P]dt}{\int S(\nu)d\nu} = \\ = \frac{\int_0^{T/2}[\nu_0(P_0 \pm \Delta P) \pm \Delta\nu_m h(t)(P_0 \pm \Delta P)]dt}{\int S(\nu)d\nu} = \\ = \frac{[\frac{T}{2}\nu_0 \pm \frac{T}{2}\Delta\nu_m < h(t) >] \cdot [P_0 \pm \Delta P]}{\int S(\nu)d\nu} \end{aligned} \tag{7}$$

To calculate the total average frequency both terms are added and the average frequency is:

$$\begin{aligned} < \nu >=< \nu_+ > + < \nu_- >= \frac{TP_0\nu_0 + T\Delta P\Delta\nu_m < h(t) >}{\int S(\nu)d\nu} = \\ = \frac{TP_0[\nu_0 + \frac{\Delta P}{P_0}\Delta\nu_m < h(t) >]}{\int S(\nu)d\nu} \end{aligned} \tag{8}$$

Where $< h(t) >= \frac{2}{T}\int_0^{T/2} h(t)dt$ and $\int S(\nu)d\nu = \int Pdt = T \cdot P_0$ and so the final average frequency is:

$$< \nu >= \nu_0 + \frac{\Delta P}{P_0}\Delta\nu_m < h(t) > \tag{9}$$

C - EXPERIMENTAL EQUIPMENT AND CONFIGURATION

Experimental equipment

Part	**Commercial name**
Laser diode	Thorlabs CLD1015
Splitter	Thorlabs TW1550RSA1
Circulator	Thorlabs 126537165
Fabry-Perot	Micron Optics Fiber FP 7447
Wave generator LD	R&S HMF2550
DC source	Siglent SPD3303C
Oscilloscope	Tektronix MSO64
Wave generator FP	Agilent 33250A
Photodiode	Thorlabs DET01CFC/M
Optical Spectrum Analyzer	MS9740B

Oscilloscope setting

Channel	**Input**	**Observations**
1	Laser output	$R_{input} = 5k\Omega$
2	Transmitted intensity through the Fabry-Perot	$R_{input} = 5k\Omega$
3	Wage generator LD signal	-
4	Wave generator FP trigger	-

D - MATLAB CODE

Code for reading OSA measurements

```
    clear %Remove previous variables
format long

%Names of data files
FN1='30mA_test5_avch1.mat';
FN2='30mA_test5_avch2.mat';

mod=FN1(1:2); %Modulation of the laser diode
ch1=load(FN1); %[V]
ch2=load(FN2); %[V]
%Change the V to I
ch1.data=ch1.data./5000; %[A]=[V]/[OHM]
ch2.data=ch2.data./5000;
%% Square wave calculation%
%% Initial data treatment
%Every modulation has a different intensity threshold and average
%wavelength

switch mod
    case '22'
        high_thrsh=10.5*1e-4;
        low_thrsh=7.57*1e-4;
        av_wave=1546.9024;
    case '24'
        high_thrsh=10.65*1e-4;
        low_thrsh=7.42*1e-4;
    case '26'
        high_thrsh=10.8*1e-4;
        low_thrsh=7.25*1e-4;
    case '28'
        high_thrsh=10.9*1e-4;
        low_thrsh=7.1*1e-4;
    case '30'
        high_thrsh=11.1*1e-4;
        low_thrsh=6.95*1e-4;
        av_wave=1546.9205;
    case '32'
        high_thrsh=11.3*1e-4;
        low_thrsh=6.8*1e-4;
```

```
40 end
41
42 %Extract values from the I_LD
43 I_0=mean(ch2.data);    %I_0: average of the whole signal
44 nI_l=ch2.data<low_thrsh;     %nI_l: Indexes of the values in ...
       the low pulse
45 nI_h=ch2.data>high_thrsh;       %nI_h: Indexes of the values ...
       in the high pulse
46 I_l=mean(ch2.data(nI_l)); %I_l: Average of the low pulse values
47 I_h=mean(ch2.data(nI_h)); %I_h: Average of the high pulse values
48 Δ_Im=I_h-I_l          %\Delta I_m: Amplitude of the intensity ...
       modulation
49 Δ_im=Δ_Im/I_0/2   %\Delta i_m: Normalized amplitude of the ...
       intensity modulation
50 %% Find low trigger locations
51
52 %Pulse locations
53 low_val=find(ch2.data<low_thrsh);
54
55 %This is to detect non-consecutive sequences, there is a peak ...
       in the sample
56 %number that is a new pulse
57 diff_low_val=diff(low_val);
58 [¬,b]=findpeaks(diff_low_val,'MinPeakHeight',3000);
59
60 %Retrieve the pulse locations and values
61 trigger_loc_l=low_val(b);                    %Locations
62 trigger_val_l=ch2.data(trigger_loc_l);  %Values
63 %% Find high trigger locations
64 %The same as the section above
65 high_val=find(ch2.data>high_thrsh);
66 diff_high_val=diff(high_val);
67 [¬,c]=findpeaks(diff_high_val,'MinPeakHeight',3000);
68 trigger_loc_h=high_val(c);
69 trigger_val_h=ch2.data(high_val(c));
70 %% Coordinate trigger high and low values
71 %Make high and low values the same length
72 b=length(trigger_loc_h);
73 c=length(trigger_loc_l);
74 if b>c
75     %c=c-1;
76     trigger_loc_h=trigger_loc_h(end-c+1:c);
77     trigger_val_h=trigger_val_h(end-c+1:c);
78     trigger_loc_l=trigger_loc_l(2:c);
79     trigger_val_l=trigger_val_l(2:c);
80 else
81     %b=b-1
82     trigger_loc_l=trigger_loc_l(end-b+1:b);
83     trigger_val_l=trigger_val_l(end-b+1:b);
84     trigger_loc_h=trigger_loc_h(2:b);
85     trigger_val_h=trigger_val_h(2:b);
86 end
87 %% i+ AND i-
88 ns=30800; %THE LENGTH OF HALF A PULSE IS 31261 (MAXIMUM)
89 % WE WANT TO LEAVE SOME SPACE WITH THE EDGES 2x"free_sp" IN ...
       TOTAL, "free_sp" EACH SIDE
90 free_sp=floor((min(trigger_loc_h-trigger_loc_l)-ns)/2);
91
```

```
92 %Empty vectors of the FP intensity
93 I_plus=zeros(ns*length(trigger_loc_l),1);
94 I_plus_av=zeros(length(trigger_loc_l),1);
95 I_minus=zeros(ns*length(trigger_loc_l),1);
96 I_minus_av=zeros(length(trigger_loc_l),1);
97 I_time=zeros(ns*length(trigger_loc_l),1);
98
99 %Temporary intensity vectors, for the loop
100 I_plus_temp=zeros(ns,1); %High pulse
101 I_minus_temp=zeros(ns,1); %Low pulse
102
103 %Time vectors, also temporary, for the loop
104 pulse_t=zeros(ns,1); %
105 t_av=zeros(length(trigger_loc_l),1); %For the averaged vectors
106
107 %Loop for every pulse
108 for e=0:length(trigger_loc_h)-1;
109
110 %Select pulses
111     pulse_h=ch1.data(trigger_loc_h(e+1)-ns-free_sp:     ...
        trigger_loc_h(e+1)-free_sp); %Single high n pulse
112     pulse_l=ch1.data(trigger_loc_l(e+1)-ns-free_sp:     ...
        trigger_loc_l(e+1)-free_sp); %Single low n pulse
113     pulse_t_h=ch1.time(trigger_loc_h(e+1)-ns-free_sp:     ...
        trigger_loc_h(e+1)-free_sp);
114     pulse_t_l=ch1.time(trigger_loc_l(e+1)-ns-free_sp:     ...
        trigger_loc_l(e+1)-free_sp); %Time vector for that pulse
115
116     %Loop to add the different values in every one
117     I_plus_temp=pulse_h+pulse_l;
118     I_minus_temp=pulse_h-pulse_l;
119
120     %We save the results and their times in a long array
121     I_plus(e*ns+1:(e+1)*ns)=I_plus_temp(1:ns);
122     I_plus_av(e+1)=mean(I_plus_temp);
123     I_minus(e*ns+1:(e+1)*ns)=I_minus_temp(1:ns);
124     I_minus_av(e+1)=mean(I_minus_temp);
125     I_time(e*ns+1:(e+1)*ns)=pulse_t_l(1:ns);
126     t_av(e+1)=pulse_t_l(ns/2);
127 end
128 %% PLOT EVERYTHING
129
130 figure()
131 plot(ch1.time,ch1.data)
132 hold on
133 plot(I_time,I_plus,'o',I_time,I_minus,'o')
134 title('I+ and I-')
135 xlabel('Time [s]')
136 ylabel('Intensity [A]')
137 legend ('I FP output','I+','I-')
138 %% Calculate L and L'
139
140 %Normalize I_plus and I_minus
141 I_plus_av_norm=I_plus_av./I_0;
142 I_minus_av_norm=I_minus_av./I_0;
143
144 %With the average
145 L_0=(I_plus_av_norm-Δ_im*I_minus_av_norm)./(2*(1-Δ_im^2));
```

```
L_0_prima=(-Δ_im*I_plus_av_norm+I_minus_av_norm)./(2*(1-Δ_im^2));

%L prima scaling
c=3e8;
nu_h_av=((c/1546.8927e-9)-(c/(av_wave*1e-9)))/(Δ_im);
L_0_prima_scaled=L_0_prima/nu_h_av;

figure()
plot(ch1.time,ch1.data)%.*1e3)
hold on
plot(t_av,L_0,'o')%,t_av,L_0_prima,'o') %average
%plot(I_time,L_0,I_time,L_0_prima) %Non-average
%title('L_0') % and L_0 prima
legend("Transmitted"+newline+ "signal",'L_0')%,'L_0 prima')
xlabel('Time [s]')
ylabel('Intensity [A]')

figure()
plot(t_av,L_0_prima_scaled)
%% Changing time to wavelength

%Cropping data
middle1=length(L_0)/2;
L_0_half=L_0(middle1:end);
L_0_prima_half=L_0_prima_scaled(middle1:end);
t_av_half=t_av(middle1:end);
%Centering cropped data
[¬,n_max]=max(L_0_half);
win=length(L_0_half)-n_max;
L_0_half=L_0_half(n_max-win:n_max+win);
L_0_prima_half=L_0_prima_half(n_max-win:n_max+win);
t_av_half=t_av_half(n_max-win:n_max+win);

%Actually changing time
middle2=floor(length(t_av_half)/2);
%Centering around 0
lambda_av_half=(t_av_half-t_av_half(middle2))*(8.8e-10/0.5)*1e12;

figure()
plot(lambda_av_half,L_0_half,'LineWidth',1.3,'Color',"#D95319")
hold on
xlabel ('Wavelength shift [pm]','FontSize',12)
ylabel('Transmission [a.u.]','FontSize',12)

figure()
plot(lambda_av_half,L_0_prima_half,'LineWidth',1.3,'Color',"#D95319")
xlabel ('Wavelength shift [pm]','FontSize',12)
ylabel('Transmission derivative [a.u.]','FontSize',12)

%% Derivative comparison
L0_prima_calc=diff(L_0_half)./diff(t_av_half);
t_av_calc=zeros(length(L0_prima_calc),1);

for e=1:length(t_av_calc)
    t_av_calc(e)=(t_av(e)+t_av(e+1))/2;
end

lambda_av_half_calc=zeros(length(L0_prima_calc),1);
```

```
204
205 for e=1:length(lambda_av_half_calc)
206     lambda_av_half_calc(e)=(lambda_av_half(e)+lambda_av_half(e+1))/2;
207 end
208
209 load('dt_dnu_1.mat');
210 load('dt_dnu_2.mat');
211
212 if mod=='22'|'24'
213     L0_prima_calc_scaled=L0_prima_calc.*dt_dnu_1;
214 else
215     L0_prima_calc_scaled=L0_prima_calc.*dt_dnu_2;
216 end
217
218 %Comparison with both
219 figure()
220 plot(lambda_av_half,L_0_prima_half,'LineWidth',1.2)
221 hold on
222 plot(lambda_av_half_calc,L0_prima_calc_scaled,'LineWidth',1.2)
223 xlabel('Wavelength shift [pm]')
224 ylabel('Transmission derivative [a.u.]')
225 legend('Method','Calculated')
226
227 %% Comparison zero-crossing
228 x0_method=(lambda_av_half(209)-lambda_av_half(208))*(-L_0_prima_half(208))/ ...
    (L_0_prima_half(209)-L_0_prima_half(208))+lambda_av_half(208);
229 x0_calc=(lambda_av_half_calc(207)- ...
    lambda_av_half_calc(206))*(-L0_prima_calc_scaled(206))    ...
    /(L0_prima_calc_scaled(207)-
230 L0_prima_calc_scaled(206))+lambda_av_half_calc(206);
231 Δ_x0=x0_method-x0_calc
```

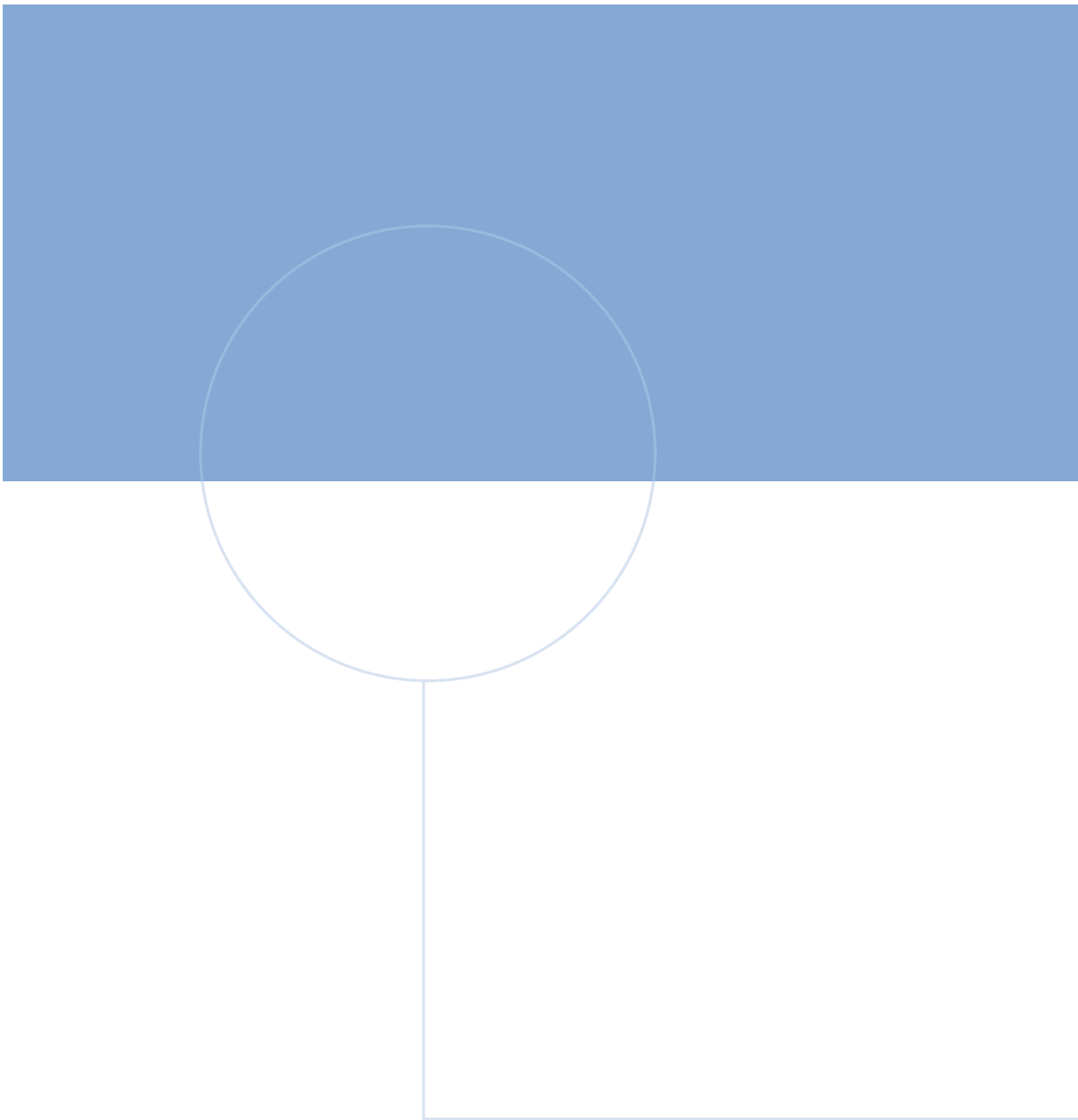

NTNU

Norwegian University of
Science and Technology